

# S<sup>2</sup>LM: Towards Semantic Steganography via Large Language Models

Huanqi Wu<sup>1</sup>, Huangbiao Xu<sup>1</sup>, Runfeng Xie<sup>2</sup>, Jiaxin Cai<sup>1</sup>, Kaixin Zhang<sup>1</sup>, Xiao Ke<sup>1\*</sup>

<sup>1</sup>College of Computer and Data Science, Fuzhou University, Fuzhou 350108, China

<sup>2</sup>College of Computer Science, Beijing University of Technology, Beijing 100124, China

wuhuanqi135@gmail.com, huangbiaoxu.chn@gmail.com, 23randomforest@gmail.com  
jiaxincai528@163.com, 241027105@fzu.edu.cn, kex@fzu.edu.cn

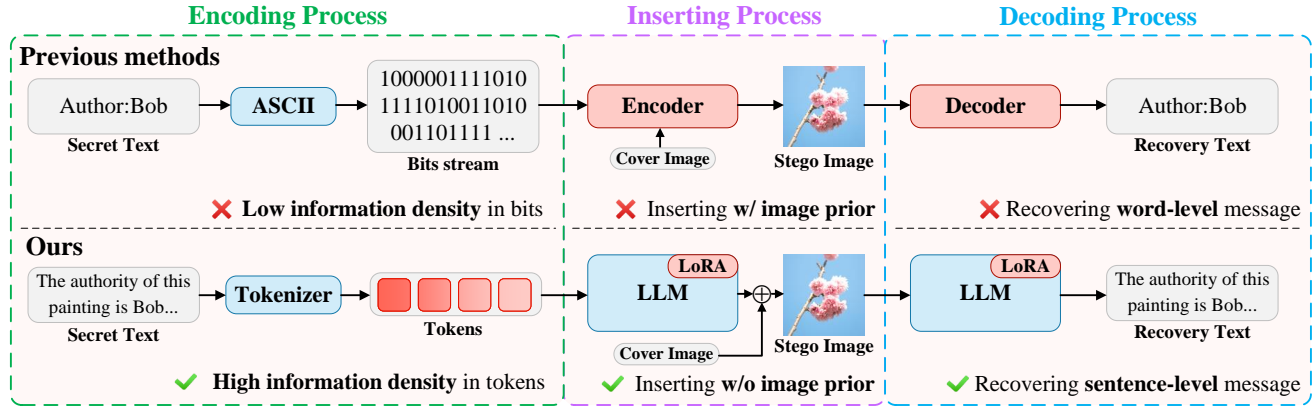


Figure 1. Overview of our S<sup>2</sup>LM framework vs. previous approaches. We define the pipeline in three processes and show the difference between the previous methods and our S<sup>2</sup>LM framework.

## Abstract

Despite remarkable progress in steganography, embedding semantically rich, sentence-level information into carriers remains a challenging problem. In this work, we present a novel concept of **Semantic Steganography**, which aims to hide semantically meaningful and structured content, such as sentences or paragraphs, in cover media. Based on this concept, we present Sentence-to-Image Steganography as an instance that enables the hiding of arbitrary sentence-level messages within a cover image. To accomplish this feat, we propose **S<sup>2</sup>LM: Semantic Steganographic Language Model**, which leverages large language models (LLMs) to embed high-level textual information into images. Unlike traditional bit-level approaches, S<sup>2</sup>LM redesigns the entire pipeline, involving the LLM throughout the process to enable the hiding and recovery of arbitrary sentences. Furthermore, we establish a benchmark named **Invisible Text (IVT)**, comprising a diverse set of sentence-level texts as secret messages to evaluate semantic steganography methods. Experimental results demonstrate that S<sup>2</sup>LM effectively enables direct sentence recovery beyond bit-level steganography. The source code and IVT dataset will be released soon.

## 1. Introduction

Steganography is the art of hiding information in plain sight. Historically, it was used as a means of covert communication during wartime. Nowadays, these techniques have found broader applications in copyright protection [79], tamper detection [78, 81], and secure communication [72].

With the advent of deep learning, steganography has achieved remarkable progress in recent years. However, despite this apparent prosperity, existing steganographic models can hide only few words of secret information. This limitation primarily arises from their design paradigm: the secret message must first be converted into a bitstream before being processed by the model. Consequently, current methods are fundamentally designed to embed binary data [9, 60, 68], which severely restricts their capacity and leads to low communication efficiency in practical applications.

For further analysis, we take image steganography as a case study and divide the steganographic pipeline into three processes, as illustrated in Fig. 1. There are three significant limitations that hinder existing methods from embedding larger amounts of information into images: 1) In the encoding process, messages are converted into bitstreams via ASCII or UTF encoding. This method is simple but primitive, neglects the semantic relationships between words, has

a low information density, and is unsuitable for encoding large amounts of information, such as sentences. 2) In the insertion process, the encoder takes the secret message and cover image as input to generate a stego image. The interaction between two fundamentally different modalities (bitstreams and images) results in suboptimal insertion performance. 3) In the decoding process, due to the aforementioned constraints, the decoder can only recover bitstreams, restricting the hidden information to the word level. These practical limitations call for a rethinking of steganography: **Are steganographic frameworks inherently limited to hiding low-level bitstream information?**

Motivated by this question, we introduce the broader concept of **Semantic Steganography**, which focuses on embedding semantically meaningful and structured content, such as natural language, into carriers. Building on this idea, we formalize the **Sentence-to-Image Steganography** task as an instance of semantic steganography. This task requires hiding sentence-level or even paragraph-level information in a cover image. Notably, the secret message can consist of arbitrary textual content of any length. To accomplish this task, the model must possess two key capabilities: encoding large and complex information into an appropriate representation and effectively handling two fundamentally different modalities.

Recent advancements in large language models (LLMs) have spurred research on integrating them with vision backbones, leading to the rise of vision-language models (VLMs) [37, 42, 43, 70, 76]. These studies demonstrate that LLMs exhibit strong capabilities in semantic understanding and cross-modal reasoning, which precisely align with the requirements of semantic steganography. This alignment highlights the potential of LLMs to serve as a foundation for developing a universal steganographic framework that embeds high-level semantics within carriers.

Building on this insight, we propose the **Semantic Steganographic Language Model (S<sup>2</sup>LM)**, a novel framework that leverages the semantic understanding capability of LLMs for steganography. To address the three challenges mentioned above, S<sup>2</sup>LM completely redesigns the entire pipeline of current methods, as illustrated in Fig. 1. 1) In the encoding process, we first transform the secret textual information into a sequence of discrete tokens using a tokenizer. This process not only captures the semantic content of the sentence but also preserves the relationships between words, enabling more effective and structured representation of the secret message. 2) During the insertion process, we leverage LLM to generate secret embeddings without relying on any prior of the cover image. By decoupling secret embeddings from the carrier, S<sup>2</sup>LM prevents potential interference between the hidden message and the cover image. 3) In the decoding process, we employ the same LLM to decode the secret message from the stego image.

Overall, S<sup>2</sup>LM provides a unified framework to handle the sentence-to-image task, demonstrating strong capability in encoding and recovering semantically rich messages without compromising visual integrity. In our qualitative experiments, S<sup>2</sup>LM successfully conceals up to  $\sim 500$  words of text into a single image with a resolution of  $256 \times 256$ , breaking the boundary between image and text. We further evaluate the steganographic performance of different LLMs within the S<sup>2</sup>LM framework and verify its versatility across various models.

Additionally, we establish a benchmark for semantic steganography called **Invisible Text (IVT)**, which we use to validate the effectiveness of the sentence-to-image framework in this paper. Overall, our contributions are as follows:

- We propose the concept of **Semantic Steganography** and formalize **Sentence-to-Image Steganography** as an instance, redefining the traditional goal of steganography from embedding low-level data to concealing meaningful language content within cover media.
- We propose the **S<sup>2</sup>LM** framework, incorporating new capabilities to embed sentence-level information into images. It demonstrates the potential of LLMs in steganography, achieving a significant increase in capacity compared to traditional methods.
- We establish a benchmark for semantic steganography named **Invisible Text (IVT)**, containing thousands of samples from diverse sources. This benchmark is essential for evaluation and encourages the community to further explore the potential of semantic steganography.

## 2. Related Work

### 2.1. Image Steganography

Steganography is a technique for concealing secret information within a carrier while preserving its visual appearance and avoiding detection. Traditional image steganography methods, such as the Least Significant Bit (LSB) algorithm [65] and frequency-domain approaches [12, 48], embed secret data by modifying the pixel values or transform coefficients of the cover image. However, these hand-crafted methods tend to introduce statistical artifacts that can be easily detected by steganalysis, whereas deep learning-based methods achieve higher security. Recent advances in deep learning have produced more powerful steganographic techniques, such as HiDeN [83], LFM [68], and StegaStamp [60], which can embed bit-level information in images with robustness against various manipulations. Moreover, methods like HiNet [29], ISN [45], LanNet [36], and StegFormer [31] offer greater capacity, enabling the concealment of an image in a carrier with the same resolution. Recently, several works have explored utilizing diffusion models for steganography, such as DGADM-GIS [73], RoSteALS [9], and Latent Watermark [46].

Despite these advancements, existing methods primarily focus on embedding secret information at a low level (bits or images). In this paper, we present a novel steganographic task, Sentence-to-Image Steganography, which aims to conceal semantically meaningful content (*e.g.*, sentence) into images. To this end, we propose S<sup>2</sup>LM, successfully embedding sentence-level textual data into cover images, significantly expanding the scope of steganography.

## 2.2. Large Language Models in Computer Vision

The prosperity of current LLMs has pushed the entire Natural Language Processing community into new boundaries. The computer vision community has also recognized the tremendous success of LLMs. Consequently, lots of the latest research focuses on exploring the integrity of the LLM with the vision backbone. BLIP [38] proposes a Multi-modal mixture of Encoder-Decoder (MED), while BLIP2 [39] introduces a frozen LLM to bootstrap vision-to-language learning, and proposes a Q-Former to bridge the modality gap. LLaVA [42] connects the vision backbone and Llama [62] and tunes the LLM with multi-modal language-image instruction-following data, achieving the general-purpose visual and language understanding.

The methods above explore the LLM application in visual understanding, often seen as a high-level vision task. However, the LLM can also enhance the performance of the low-level vision backbone. LISA [35] uses a novel segmentation token and unlocks the segmentation capability of the LLM, which can be used for reasoning segmentation tasks. Xu *et al.* used localized image captioning data to pre-train PixelLLM to equip it with localization capability [69]. Zheng *et al.* froze LLM to solve a range of low-level vision tasks, demonstrating the LLM’s strong generalization capability [82].

While several studies have attempted to apply LLMs to linguistic steganography [5, 54, 66], most of them rely on manually designed sampling strategies. In this paper, we integrate LLM into the entire steganographic pipeline, directly utilizing LLM to generate secret embeddings directly, and successfully scale the steganographic capacity from bit to sentence-level.

## 3. Semantic Steganography

The whole steganographic community has traditionally focused on low-level information hiding (*e.g.*, at the bit or image level), overlooking the semantic structure of the hidden information. In contrast, we introduce a new direction of **Semantic Steganography**, which refers to hiding semantically meaningful and structured content, such as sentences or paragraphs, in the carrier. This paradigm redefines what kind of information can be hidden. Rather than merely embedding arbitrary bitstreams, it enables the direct hiding and recovery of natural language messages, which benefits

the steganographic techniques by expanding their expressive and potential use cases.

### 3.1. Problem Definition

We define semantic steganography as the task of hiding semantic content within a carrier while keeping it undetectable. In this work, the semantic content of interest is expressed in natural language, specifically as complete sentences that convey coherent and interpretable meaning.

Formally, let  $m$  denote a natural language message, and  $O_{\text{cover}}$  denote a cover object. The encoder  $E(\cdot)$  embeds  $m$  into  $O_{\text{cover}}$ , producing the stego object  $O_{\text{stego}} = E(O_{\text{cover}}, m)$ . The corresponding decoder  $D(\cdot)$  aims to recover the original message as  $\hat{m} = D(O_{\text{stego}})$ . The semantic steganography task must satisfy the following constraints:

$$\begin{cases} \text{Recoverability:} & S(\hat{m}, m) \rightarrow 1, \\ \text{Imperceptibility:} & \Delta(O_{\text{cover}}, O_{\text{stego}}) \leq \epsilon, \\ \text{Security:} & P(O_{\text{stego}}) \approx P(O_{\text{cover}}). \end{cases} \quad (1)$$

Specifically, recoverability measures the semantic consistency of the recovery message using the similarity function  $S$ . Imperceptibility evaluates the similarity between cover and stego objects, where  $\Delta(\cdot, \cdot)$  measures perceptual distortion, and  $\epsilon$  denotes the maximum allowable perceptual difference. Security reflects the indistinguishability between cover and stego objects against steganalysis.  $P(\cdot)$  represents the output of the steganalysis tool.

In essence, semantic steganography generalizes the notion of information hiding from the signal level to the semantic level. By encoding linguistic meaning rather than raw bits, it establishes a unified framework for embedding natural language semantics across arbitrary modalities.

### 3.2. Benchmark

However, there is an absence of datasets specially designed for evaluating semantic steganography. To fill this gap, we construct the **Invisible Text (IVT)** dataset, which comprises a diverse set of sentence-level texts drawn from existing text datasets and generated by LLMs, serving as secret messages. We divide the messages into three levels of granularity: short messages (one sentence), medium messages (two to three sentences), and long messages (full articles), denoted as IVT-S, IVT-M, and IVT-L, respectively. Please refer to Sec. 7 of supplementary materials for more details.

### 3.3. Sentence-to-Image Steganography

Specifically, we formalize the sentence-to-image steganography task as a concrete instantiation of the semantic steganography. Following the definition above, the object  $O$  in this task is specified as an image  $I$ . The objective is to secretly embed natural-language messages within the image while ensuring that the hidden information can be accurately recovered.

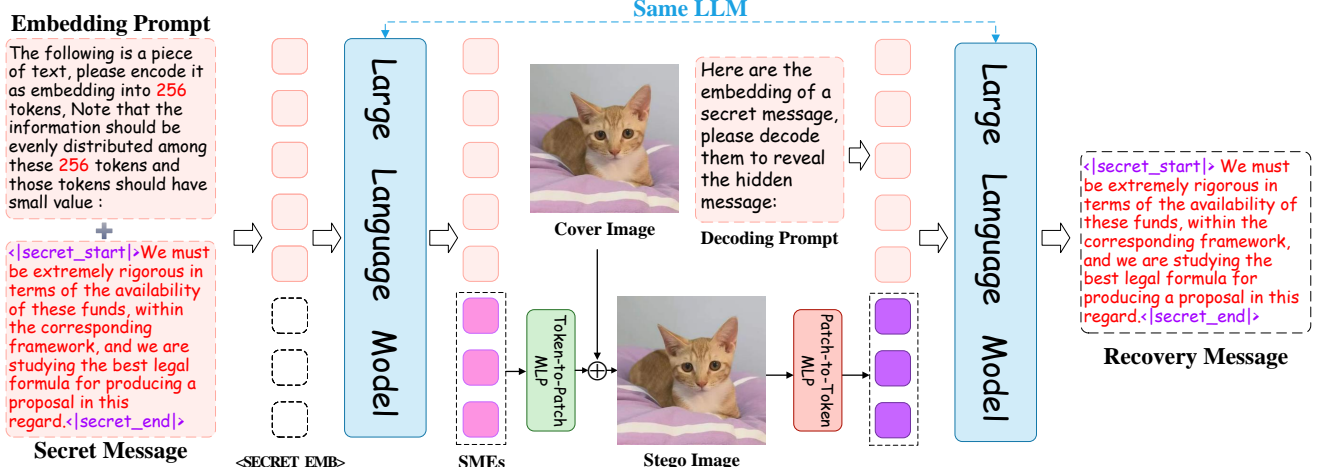


Figure 2. The pipeline of the S<sup>2</sup>LM framework.

## 4. Method

### 4.1. Representing Information as Tokens

The representation of secret message is a critical aspect of semantic steganography. Previous methods convert each character of a word into bits using UTF encoding[60, 68, 83]. However, such character-level representations have two significant limitations. First, UTF encoding lacks semantic compression capability, treating each character equally regardless of its meaning. Second, encoding a sentence as a bitstream leads to an excessively long sequence that is difficult to process. We hypothesize that such primitive representations are fragile when encoding richer semantic content. Therefore, it is necessary to explore more effective representations for sentence-level information.

To address these issues, we leverage the tokenizer to convert the secret sentence into tokens. Tokenization [67] is a widely used technique in NLP, where sentences are broken down into smaller units called **Tokens**. Unlike character-level encoding, tokens correspond to semantically meaningful units, such as words, sub-words, or phrases, allowing a more compact representation. This not only preserves the semantic structure of the sentence but also significantly shortens the sequence length, improving the efficiency and stability of downstream embedding and decoding processes.

### 4.2. LLMs for Steganography

As shown in Fig. 2, the S<sup>2</sup>LM consists of three key modules: a pre-trained LLM for embedding and decoding the secret information, a Token-to-Patch MLP  $\mathcal{F}_{T2P}$  for aligning text features and image features, and a Patch-to-Token MLP  $\mathcal{F}_{P2T}$  for embedding visual features to token embeddings. Notably, S<sup>2</sup>LM is a universal framework in which the LLM can be **ANY** pre-trained LLM.

**Semantic Embedding via LLMs.** The LLM is recognized

as the *de facto* standard architecture in the NLP community. Recent studies, however, have demonstrated that LLM can serve as a universal interface with different instructions in language to complete different tasks. In the computer vision community, researchers have explored integrating LLMs with vision backbones for segmentation [35], grounding [30, 50, 69], and other visual tasks [74]. Inspired by these works, we employ an LLM to generate embeddings conditioned by secret information, which will be inserted into the cover image to produce the stego image. Owing to the strong generalization ability of LLMs, we are able to compress the semantic information into a few embeddings.

Specifically, as illustrated in Fig. 2, we design an embedding prompt  $X_{prompt}^{embed}$  and concatenate it with a secret message to instruct the LLM to embed the secret message into embeddings, which we call secret message embeddings (SMEs). We call this strategy **Prompt-Guide Embedding**. The SMEs are then aligned with the image feature using the  $\mathcal{F}_{T2P}$ . After that, we reshape it and add to the cover image to get a stego image.

**Universal Insertion.** To insert SMEs into the cover image, we use  $\mathcal{F}_{T2P}$  to align the token embeddings with the image features. Then, we adapt the UDH method [75], which directly adds the SMEs to the cover image to produce a stego image. Previous methods generate the stego image conditioned on both the cover image and the secret message. Empirically, however, the UDH method decouples the secret message from the carrier, resulting in smoother training and improved performance.

**Decoding via LLMs.** After receiving the stego image, we reshape it in patches and use  $\mathcal{F}_{P2T}$  to extract features and concatenate it with decoding prompt  $X_{prompt}^{decode}$ , which is used to instruct the LLM to decode the secret message. Finally, we get the recovery message from the LLM.

**Template Designing.** As illustrated in Fig. 3, we care-

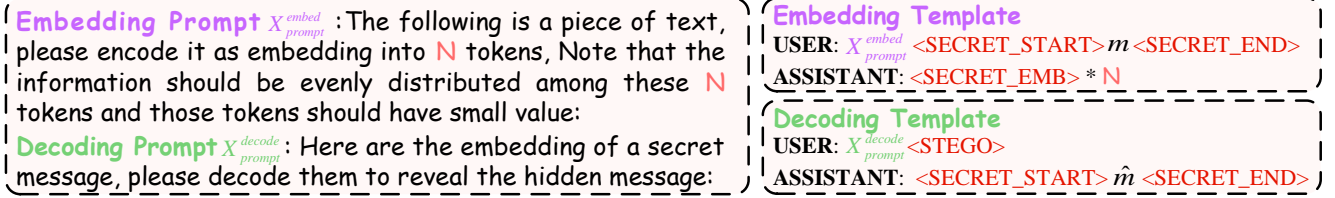


Figure 3. Prompt templates used in the embedding and decoding procedures of  $S^2LM$ .



Figure 4. Two-stage training strategy for  $S^2LM$ .

fully design the embedding and decoding prompts to instruct the LLM to embed and recover the secret message. We introduce two special tokens:  $\langle SECRET\_START \rangle$  and  $\langle SECRET\_END \rangle$ , which are used to separate secret messages from the prompt. We use the output embeddings of the LLM as SMEs. For clarity, we denote the location of the SMEs in the output of LLM as  $\langle SECRET\_EMB \rangle$ . During the decoding process, the extracted feature will be concatenated with the decode prompt as the input of LLM. We use  $\langle STEGO \rangle$  as the placeholder for the feature extracted from stego image by  $\mathcal{F}_{T2P}$ .

### 4.3. Training of $S^2LM$

**Trainable Parameters.** To preserve the knowledge of the LLM, we use LoRA [26] for fine-tuning. Additionally, because we introduce new tokens into the vocabulary (e.g.  $\langle SECRET\_START \rangle$ ), we also set the LLM token embeddings (*embed\_tokens*) and the LLM head (*lm\_head*) trainable. By the way, the  $\mathcal{F}_{T2P}$  and  $\mathcal{F}_{P2T}$  are also trainable.

**Stage 1: Pre-Training for Steganography.** As shown in Fig. 4, the  $S^2LM$  training process consists of two stages. In the first stage, we train the LLM (with LoRA), together with  $\mathcal{F}_{T2P}$  and  $\mathcal{F}_{P2T}$ . In this stage, we **DO NOT** introduce the cover image. We wrap the secret message  $m$  with  $\langle SECRET\_START \rangle$  and  $\langle SECRET\_END \rangle$  to construct the input sequence  $M$ :

$$M = \langle SECRET\_START \rangle \parallel m \parallel \langle SECRET\_END \rangle. \quad (2)$$

Given the embedding prompt  $X_{prompt}^{embed}$  along with  $M$ , we feed them into the LLM, which outputs a response token sequence  $Y_{res}$ , which can be formulated as:

$$Y_{res} = LLM(X_{prompt}^{embed}, M). \quad (3)$$

We extract the last-layer embedding  $e \in \mathbb{R}^{N \times d_{emb}}$  of the LLM as the secret embedding corresponding to the  $\langle SECRET\_EMB \rangle$  token in  $Y_{res}$  and apply  $\mathcal{F}_{T2P}$  to obtain

$p \in \mathbb{R}^{N \times d_{patch}}$ , which aligns with the image patch dimension. Subsequently,  $p$  will be processed by  $\mathcal{F}_{P2T}$  to align with the token embedding dimension of the LLM, yielding  $e' \in \mathbb{R}^{N \times d_{emb}}$ . To prevent the LLM from focusing solely on a subset of embeddings, we randomly mask  $e'$  with a mask ratio  $R$ , which we refer to as the **Mask Strategy**. Finally, we concatenate it with decode prompt  $X_{prompt}^{decode}$  and feed it into the LLM to obtain the recovery message  $\hat{M}$ , which can be formulated as:

$$\begin{aligned} p &= \mathcal{F}_{T2P}(e), \quad e' = \mathcal{F}_{P2T}(p), \\ \hat{M} &= LLM(X_{prompt}^{decode}, \text{Mask}(e', R)). \end{aligned} \quad (4)$$

**Stage 2: Fine-Tuning on Stego Images.** In the second stage, we **FREEZE** the LLM and  $\mathcal{F}_{P2T}$ , **TRAIN**  $\mathcal{F}_{T2P}$ , and introduce the cover image  $I_{cover} \in \mathbb{R}^{C \times H \times W}$ . After obtaining  $p \in \mathbb{R}^{N \times d_{patch}}$ , we reshape it from patch representation to the image representation  $I_{emb} \in \mathbb{R}^{C \times H \times W}$ , and add it to  $I_{cover}$  to obtain stego image  $I_{stego}$ . The entire process can be formulated as follows:

$$\begin{aligned} I_{emb} &= \text{Reshape}(p), \\ I_{stego} &= I_{cover} + I_{emb}. \end{aligned} \quad (5)$$

After receiving the stego image, we divide it into patches to transform it into a 1D sequence  $\hat{p} \in \mathbb{R}^{N \times d_{patch}}$  and feed it into  $\mathcal{F}_{P2T}$  to obtain  $\hat{e} \in \mathbb{R}^{N \times d_{emb}}$ . Finally, we concatenate decode prompt  $X_{prompt}^{decode}$  with the  $\hat{e}$  and feed it into the LLM to get the recovery message  $\hat{M}$ , which can be formulated as follows:

$$\begin{aligned} \hat{p} &= \text{Patchify}(I_{stego}), \quad \hat{e}' = \mathcal{F}_{P2T}(\hat{p}), \\ \hat{M} &= LLM(X_{prompt}^{decode}, \hat{e}'). \end{aligned} \quad (6)$$

**Training Objectives.** The  $S^2LM$  is trained using the text generation loss  $\mathcal{L}_{txt}$  and the embedding loss  $\mathcal{L}_{emb}$ . The overall objective  $\mathcal{L}$  of each stage is defined as the weighted sum of these losses:

$$\begin{aligned} \mathcal{L}_{\text{stage-1}} &= \lambda_{txt} \mathcal{L}_{txt} + \lambda_{emb} \mathcal{L}_{emb}, \\ \mathcal{L}_{\text{stage-2}} &= \lambda_{txt} \mathcal{L}_{txt}. \end{aligned} \quad (7)$$

Table 1. Quantitative results on the IVT-S, IVT-M, and IVT-L benchmarks.

Methods	IVT-S						IVT-M						IVT-L					
	Secret/Recovery			Cover/Stego			Secret/Recovery			Cover/Stego			Secret/Recovery			Cover/Stego		
	WER	BLEU	ROUGE	BERT-S	PSNR	SSIM	WER	BLEU	ROUGE	BERT-S	PSNR	SSIM	WER	BLEU	ROUGE	BERT-S	PSNR	SSIM
StegaStamp [60]	0.452	0.241	0.138	0.347	35.6	0.927	-	-	-	-	-	-	-	-	-	-	-	-
DwtDct [12]	0.007	0.899	0.996	<b>0.996</b>	31.8	0.898	0.701	0.490	0.713	0.429	27.7	0.776	-	-	-	-	-	-
FPGP [80]	0.150	0.882	0.925	0.914	43.5	0.954	0.758	0.462	0.539	0.538	35.6	0.874	-	-	-	-	-	-
LanNet [36]	0.004	<b>0.906</b>	<b>0.997</b>	<b>0.996</b>	42.1	0.951	0.244	0.698	0.836	0.787	41.3	0.949	0.824	0.031	0.288	0.630	40.9	0.941
CRMark [10]	<b>0.003</b>	0.904	0.994	0.994	<b>47.3</b>	0.985	0.185	0.724	0.862	0.894	40.5	0.914	0.806	0.142	0.305	0.683	37.6	0.825
S <sup>2</sup> LM-Qwen2.5-0.5B	0.045	0.818	0.873	0.919	40.1	0.956	<b>0.043</b>	<b>0.939</b>	<b>0.974</b>	0.952	38.6	0.973	<b>0.084</b>	<b>0.903</b>	<b>0.944</b>	<b>0.945</b>	38.3	0.927
S <sup>2</sup> LM-MiniCPM-1B	0.046	0.844	0.923	0.959	41.6	0.970	<b>0.091</b>	0.889	<b>0.956</b>	<b>0.953</b>	41.4	0.969	0.172	0.801	0.874	0.900	41.0	<b>0.971</b>
S <sup>2</sup> LM-Llama3.2-1B	0.142	0.837	0.892	0.939	<b>44.9</b>	<b>0.987</b>	0.095	<b>0.918</b>	0.950	0.952	<b>45.0</b>	<b>0.987</b>	0.109	<b>0.883</b>	<b>0.922</b>	<b>0.933</b>	<b>41.9</b>	0.962
S <sup>2</sup> LM-Gemma3-1B	0.100	0.801	0.746	0.834	42.4	0.973	<b>0.091</b>	0.889	0.832	<b>0.956</b>	41.4	0.969	0.211	0.807	0.880	0.887	36.5	0.915

Specifically,  $\mathcal{L}_{txt}$  is the cross-entropy (CE) loss for text generation, and  $\mathcal{L}_{emb}$  is the L1 loss, which encourages the model to introduce minimal artifacts in the cover image. Those losses can be formulated as:

$$\mathcal{L}_{txt} = \text{CE}(\hat{M}, M), \quad \mathcal{L}_{emb} = \text{L1}(p, 0). \quad (8)$$

## 5. Experiments

### 5.1. Experimental Settings

**Model Variants.** S<sup>2</sup>LM is a universal framework compatible with any pre-trained LLM. In this paper, we instantiate it with four models: Llama3.2-1B [21], Qwen2.5-0.5B [55], Gemma3-1B [61], and MiniCPM-1B [28]. We chose edge-deployable language models with parameters fewer than 1B, which guarantees lightweight operation while maintaining the scalability to larger models.

**Implementation Details.** We employ AdamW optimizer [44]. The weights  $\lambda_{txt}$  and  $\lambda_{emb}$  are set to 1.0 and 1.0, respectively. More details can be found in Sec. 8.2 of the supplementary material.

**Datasets.** For the secret message, we use Wanjuan 1.0 [25], a comprehensive corpus designed for large language model pre-training. We randomly select 320,000 samples with fewer than 1,000 words as secret messages for training. For the cover image, we use the COCO training dataset [41]. Please refer to the supplementary material for detailed information about the training dataset. We evaluate the performance of steganographic models on the sentence-to-image steganography task, using the IVT dataset as secret messages and the COCO test dataset as cover images. For more details about IVT, please refer to Sec. 7 in the supplementary material.

**Evaluation Metrics.** The performance of the steganographic model is evaluated from three complementary perspectives: **recoverability**, **imperceptibility**, and **security**. For recoverability, we evaluate the recovery text using Word Error Rate (WER), BLEU-4 [47], ROUGE-L [40], and BERT-Score [77], which jointly assess lexical accuracy and semantic consistency. For imperceptibility, we adopt PSNR

and SSIM to measure the visual similarity between the cover and stego images. For security, we employ state-of-the-art steganalysis tools including SRNet [8], SiaSigNet [71], and DBS2Net [27], to quantify the detectability of stego images.

**Baselines.** We compare S<sup>2</sup>LM with different methods, including DwtDct [11], StegaStamp [60], LanNet [36], CRMark [10], and FPGP [80].

### 5.2. Sentence-to-Image Steganography Results

Sentence-to-Image results are shown in Tab. 1. Notably, while existing methods struggle with this task, our S<sup>2</sup>LM demonstrates strong performance.

**Results of Existing Methods.** Existing methods are not suitable for the sentence-to-image steganography task, which fundamentally differs in that it requires encoding a substantial amount of semantic information. As shown in Tab. 1, StegaStamp fails to recover secret messages in IVT-S, while DwtDct and FPGP perform well only on IVT-S, but fail to recover messages in IVT-M, not to mention handling IVT-L. However, LanNet and CRMark also fail on IVT-L.

To ensure sufficient capacity for the IVT dataset, we retrain all of the baselines and increase their steganographic capacity for each IVT dataset. However, we observe a severe mode collapse problem, which is consistent with the phenomenon reported in [52]. We provide a detailed analysis in Sec. 12.2 of the supplementary material. This issue primarily stems from limitations in the architectural design and bitstream representation of secret information. As a result, these models are restricted to hiding bit-level information and cannot handle semantic-level content, such as sentences.

**Results of S<sup>2</sup>LM.** Existing methods fail to address this task effectively, whereas S<sup>2</sup>LM successfully handles secret messages containing complex and semantically rich natural language information.

On the IVT-S, all four S<sup>2</sup>LM variants demonstrate competitive performance compared to traditional baselines in secret recovery while significantly outperforming them in the visual quality of the stego image. Specifi-



Figure 5. Qualitative results of  $S^2LM$ -Qwen2.5-0.5B on different length of secret messages.

Table 2. Results of  $S^2LM$ -Qwen2.5-0.5B on  $128 \times 128$  cover images with different secret lengths.

Capacity (Token)	Compress Ratio	Secret / Recovery				Cover / Stego	
		WER	BLEU-4	ROUGE-L	BERT-Score	PSNR	SSIM
32	1:2	0.033	0.947	0.975	0.971	34.6	0.875
64	1:1	0.035	0.952	0.977	0.969	31.6	0.773
128	2:1	0.085	0.892	0.947	0.934	33.5	0.853
256	4:1	0.214	0.725	0.860	0.858	32.4	0.809
512	8:1	0.875	0.237	0.474	0.708	31.5	0.770

ally,  $S^2LM$ -MiniCPM-1B achieves the best overall performance, while  $S^2LM$ -Qwen2.5-0.5B,  $S^2LM$ -Llama3.2-1B, and  $S^2LM$ -Gemma3-1B also deliver competitive results.

On the IVT-M, which involves longer and more complex messages, our  $S^2LM$  variants significantly outperform prior methods.  $S^2LM$ -Qwen2.5-0.5B achieves the best recovery performance among all variants while maintaining high visual quality.  $S^2LM$ -MiniCPM-1B and  $S^2LM$ -Gemma3-1B exhibit comparable performance.

On the IVT-L, all models exhibit performance degradation compared to their results on IVT-M.  $S^2LM$ -Qwen2.5-0.5B get the top recovery performance,  $S^2LM$ -MiniCPM-1B and  $S^2LM$ -Llama3.2-1B demonstrate moderate performance declines, and  $S^2LM$ -Gemma3-1B exhibits the lowest semantic accuracy.

Experimental results demonstrate that all  $S^2LM$  variants achieve strong performance on both IVT-S and IVT-M. However, for these models, IVT-L remains challenging, which comprises multi-sentence structures characterized by complex syntactic patterns and diverse lexical content. Additional robustness experiments demonstrate that  $S^2LM$  ex-

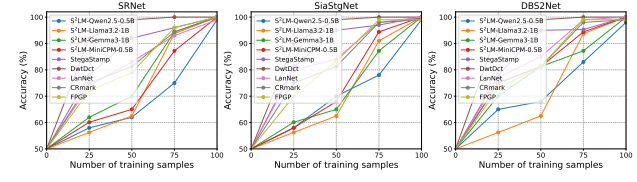


Figure 6. The results of the deep learning based steganalysis. Note that the closer the accuracy is to 50%, the stronger its resistance to steganalysis.

hibits strong resistance to various attacks while maintaining a remarkably high capacity. More details can be found in Sec. 12.4 of the supplementary material.

**Qualitative Results.** As depicted in Fig. 5, we provide a visualization of stego images and recovery results of  $S^2LM$ -Qwen2.5-0.5B in different lengths of information. We mark the difference in red. As we can see, the recovery message and the ground truth keep a high semantic similarity, while the stego image still has a good visual quality. More samples can be found in Sec. 15 of the supplementary material.

### 5.3. Capacity Analysis

In this section, we conduct empirical experiments to investigate the capacity of the cover image under the  $S^2LM$  framework. We analyze the capacity in terms of tokens, setting the secret message length to 32, 64, 128, 256, and 512 tokens, while fixing the cover image resolution at  $128 \times 128$ . We train  $S^2LM$ -Qwen2.5-0.5B from scratch for each setting. The cover image is divided into 64 patches, which is equal to the number of SMEs. For more precise analysis, we define the compression ratio as the number of message

Table 3. Ablation study of the module in the S<sup>2</sup>LM framework.

No.	Two-Stage Training	Prompt	Embedding Loss	Mask Strategy	Secret / Recovery				Cover / Stego	
					WER	BLEU-4	ROUGE-L	BERT-S	PSNR	SSIM
1					0.3162	0.5925	0.6781	0.6816	34.13	0.8156
2	✓				0.2210	0.6819	0.7403	0.8051	32.93	0.8460
3	✓	✓			0.2200	0.7319	0.7965	0.8295	31.41	0.8248
4	✓	✓	✓		0.2139	0.5676	0.6606	0.7465	<b>45.25</b>	<b>0.9839</b>
5		✓	✓	✓	0.2379	0.6703	0.7496	0.8119	34.24	0.7820
6	✓	✓	✓	✓	<b>0.0839</b>	<b>0.9028</b>	<b>0.9435</b>	<b>0.9453</b>	38.30	0.9266

tokens divided by the number of patches.

As illustrated in Tab. 2, the model maintains strong decoding performance for message lengths ranging from 32 to 256 tokens, with BERT-Scores above 0.8. However, at 512 tokens, frequent decoding errors emerge. These results indicate that while the S<sup>2</sup>LM has the information compression ability, its capacity saturates beyond a certain threshold, leading to a noticeable degradation in recovery quality.

Based on these empirical findings, we propose a practical heuristic: each image patch can stably carry approximately four tokens without significant loss in decoding fidelity. This guideline provides an interpretable measure of capacity for future designs and scaling strategies, offering a concrete reference point for balancing payload and image quality in sentence-to-image steganography.

#### 5.4. Steganalysis

Following previous works [23, 29, 31, 75, 83], we gradually increase the number of training samples to investigate the minimum number of leaking samples required to train steganalysis models for detecting stego images. We retain the SRNet, SiaStegNet, and DBS2Net with cover/stego image pairs on the COCO dataset. As shown in Fig. 6, with the increasing number of training samples, the S<sup>2</sup>LM still achieves lower detection accuracy. More details about the statistical steganalysis can be found in Sec. 9 of the supplementary material.

#### 5.5. Ablation Study

In this section, we conduct extensive ablation studies on S<sup>2</sup>LM-Qwen2.5-0.5B in the IVT-L to reveal the contribution of each component.

**Effectiveness of Two-Stage Training.** Without the two-stage training strategy, the S<sup>2</sup>LM struggles to recover the secret message (**No.1** vs. **No.2**, **No.5** vs. **No.6**). That may be because introducing the image modality at an early stage disrupts the LLM to learn steganographic mechanisms.

**Effectiveness of the Prompt.** In this experiment, we do not use prompts to guide the LLM during the embedding and decoding processes. During embedding, we simply tokenize the secret message and input it into the LLM to ob-

tain SMEs. Similarly, during decoding, we directly feed the features extracted by the Patch-to-Token MLP into the LLM to recover the original message. Comparing experiments **No.2** and **No.3** reveals that this approach leads to performance improvements of **7.3%**, **7.5%**, and **3.0%** in BLEU-4, ROUGE-L, and BERT-Score, respectively. These results confirm that the prompt effectively guides the LLM in understanding and executing the sentence-to-image task.

**Effectiveness of Embedding Loss.** A comparison between experiments **No.3** and **No.4** reveals the contribution of  $\mathcal{L}_{emb}$ .  $\mathcal{L}_{emb}$  is used to encourage the LLM to produce minimal artifacts in the cover image and is applied only in the first stage. The experimental results show that the introduction of  $\mathcal{L}_{emb}$  can improve the embedding quality, with gains of **15.61 dB** and **0.165** in the PSNR and SSIM.

**Effectiveness of Mask Strategy.** In the decoding process of the first stage, we mask some input tokens to encourage the LLM to distribute information across the entire cover image. As shown by the comparison between experiments **No.4** and **No.6**, this strategy leads to significant improvements in recovery quality. We visualize the SMEs in Sec. 11.1 of the supplementary material, which shows that the SMEs are evenly distributed with the mask strategy.

## 6. Conclusion

In this work, we propose a novel concept of semantic steganography, which aims to hide high-level semantic information in carriers and redefines the traditional paradigm of steganography. Building on this insight, we present sentence-to-image steganography as an instance, which focuses on embedding sentence-level information into images. To achieve this task, we propose S<sup>2</sup>LM, a novel steganographic framework that leverages LLMs to embed sentence-level information into images, achieving a feat that previously has been out of reach. Additionally, we present an evaluation benchmark, Invisible Text (IVT), comprising a diverse set of sentence-level texts drawn from existing datasets and generated by LLMs. We hope our work sheds new light on the advancement of semantic steganography for the entire community.

## References

- [1] Bob Adams. Southparkdata: South park scripts dataset, 2017. Dataset hosted on GitHub. [1](#), [2](#), [3](#)
- [2] Ross J Anderson and Fabien AP Petitcolas. On the limits of steganography. *IEEE Journal on selected areas in communications*, 16(4):474–481, 2002. [11](#)
- [3] Xiang Ao, Xiting Wang, Ling Luo, Ying Qiao, Qing He, and Xing Xie. PENS: A dataset and generic framework for personalized news headline generation. In *Proceedings of the 59th Annual Meeting of the Association for Computational Linguistics and the 11th International Joint Conference on Natural Language Processing (Volume 1: Long Papers)*, pages 82–92, Online, 2021. Association for Computational Linguistics. [1](#), [2](#), [3](#)
- [4] Nabiha Asghar. Yelp dataset challenge: Review rating prediction. *arXiv preprint arXiv:1605.05362*, 2016. [3](#)
- [5] Minhao Bai, Jinshuai Yang, Kaiyi Pang, Yongfeng Huang, and Yue Gao. Semantic steganography: A framework for robust and high-capacity information hiding using large language models. *arXiv preprint arXiv:2412.11043*, 2024. [3](#)
- [6] Benedikt Boehm. StegExpose - a tool for detecting lsb steganography. *ArXiv*, abs/1410.6656, 2014. [4](#)
- [7] Ondrej Bojar, Christian Buck, Christian Federmann, Barry Haddow, Philipp Koehn, Johannes Leveling, Christof Monz, Pavel Pecina, Matt Post, Herve Saint-Amand, Radu Soricut, Lucia Specia, and Ale s Tamchyna. Findings of the 2014 workshop on statistical machine translation. In *Proceedings of the Ninth Workshop on Statistical Machine Translation*, pages 12–58, Baltimore, Maryland, USA, 2014. Association for Computational Linguistics. [3](#)
- [8] Mehdi Boroumand, Mo Chen, and Jessica J. Fridrich. Deep residual network for steganalysis of digital images. *IEEE Transactions on Information Forensics and Security*, 14: 1181–1193, 2019. [6](#)
- [9] Tu Bui, Shruti Agarwal, Ning Yu, and John Collomosse. Rosteals: Robust steganography using autoencoder latent space. In *Proc. CVPR WMF*, 2023. [1](#), [2](#)
- [10] Jiale Chen, Wei Wang, Chongyang Shi, Li Dong, and Xiping Hu. Learning robust image watermarking with lossless cover recovery. In *Proceedings of the IEEE/CVF International Conference on Computer Vision*, pages 15056–15065, 2025. [6](#), [4](#), [7](#)
- [11] Kuanchin Chen. Digital watermarking and steganography. 2009. [6](#)
- [12] Po-Yueh Chen, Hung-Ju Lin, et al. A dwt based approach for image steganography. *International Journal of Applied Science and Engineering*, 4(3):275–290, 2006. [2](#), [6](#)
- [13] Thomas Davidson, Dana Warmsley, Michael Macy, and Ingmar Weber. Automated hate speech detection and the problem of offensive language. In *Proceedings of the 11th International AAAI Conference on Web and Social Media*, pages 512–515, 2017. [3](#)
- [14] DeepSeek. Deepseek chat, 2024. Large language model developed by DeepSeek. [2](#), [5](#)
- [15] Ronen Eldan and Yuanzhi Li. Tinystories: How small can language models be and still speak coherent english? *arXiv preprint arXiv:2305.07759*, 2023. [2](#), [3](#)
- [16] Ashkan Farhangi, Ning Sui, Nan Hua, Haiyan Bai, Arthur Huang, and Zhishan Guo. Protoformer: Embedding prototypes for transformers. In *Advances in Knowledge Discovery and Data Mining: 26th Pacific-Asia Conference, PAKDD 2022, Chengdu, China, May 16–19, 2022, Proceedings, Part I*, pages 447–458, 2022. [1](#), [2](#), [3](#)
- [17] Hewlett Foundation. Automated student assessment prize - automated essay scoring (asap-aes) dataset, 2012. Dataset hosted on Kaggle. [3](#)
- [18] Wikimedia Foundation. Wikimedia downloads. [2](#), [3](#)
- [19] Jessica Fridrich. *Steganography in digital media: principles, algorithms, and applications*. Cambridge university press, 2009. [10](#), [11](#)
- [20] Alec Go, Richa Bhayani, and Lei Huang. Twitter sentiment classification using distant supervision. *CS224N project report, Stanford*, 1(12):2009, 2009. [1](#), [2](#)
- [21] Aaron Grattafiori, Abhimanyu Dubey, Abhinav Jauhri, Abhinav Pandey, Abhishek Kadian, Ahmad Al-Dahle, Aiesha Letman, Akhil Mathur, Alan Schelten, Alex Vaughan, et al. The llama 3 herd of models. *arXiv e-prints*, pages arXiv–2407, 2024. [6](#), [3](#)
- [22] Jian Guan, Ziqi Liu, and Minlie Huang. A corpus for understanding and generating moral stories. *arXiv preprint arXiv:2204.09438*, 2022. [2](#), [3](#)
- [23] Zhenyu Guan, Junpeng Jing, Xin Deng, Mai Xu, Lai Jiang, Zuxun Zhang, and Yipeng Li. Deepmih: Deep invertible network for multiple image hiding. *IEEE Transactions on Pattern Analysis and Machine Intelligence*, 45:372–390, 2022. [8](#)
- [24] Frank Hartung and Martin Kutter. Multimedia watermarking techniques. *Proceedings of the IEEE*, 87(7):1079–1107, 2002. [11](#)
- [25] Conghui He, Zhenjiang Jin, Chaoxi Xu, Jiantao Qiu, Bin Wang, Wei Li, Hang Yan, Jiaqi Wang, and Da Lin. Wanjuan: A comprehensive multimodal dataset for advancing english and chinese large models. *ArXiv*, abs/2308.10755, 2023. [6](#), [2](#)
- [26] Edward J Hu, Yelong Shen, Phillip Wallis, Zeyuan Allen-Zhu, Yuanzhi Li, Shean Wang, Lu Wang, Weizhu Chen, et al. Lora: Low-rank adaptation of large language models. *ICLR*, 1(2):3, 2022. [5](#)
- [27] Mingzhi Hu and Hongxia Wang. Lightweight jpeg image steganalysis using dilated blind-spot network. *Journal of Visual Communication and Image Representation*, 101: 104182, 2024. [6](#)
- [28] Shengding Hu, Yuge Tu, Xu Han, Chaoqun He, Ganqu Cui, Xiang Long, Zhi Zheng, Yewei Fang, Yuxiang Huang, Weilin Zhao, et al. Minicpm: Unveiling the potential of small language models with scalable training strategies. *arXiv preprint arXiv:2404.06395*, 2024. [6](#), [3](#)
- [29] Junpeng Jing, Xin Deng, Mai Xu, Jianyi Wang, and Zhenyu Guan. Hinet: Deep image hiding by invertible network. In *Proceedings of the IEEE/CVF international conference on computer vision*, pages 4733–4742, 2021. [2](#), [8](#)
- [30] Seil Kang, Jinyeong Kim, Junhyeok Kim, and Seong Jae Hwang. Your large vision-language model only needs a few attention heads for visual grounding. In *Proceedings of the*

*Computer Vision and Pattern Recognition Conference*, pages 9339–9350, 2025. 4

[31] Xiao Ke, Huanqi Wu, and Wenzhong Guo. Stegformer: rebuilding the glory of autoencoder-based steganography. In *Proceedings of the AAAI Conference on Artificial Intelligence*, pages 2723–2731, 2024. 2, 8

[32] Charles Kelly. Tab-delimited bilingual sentence pairs from the tatoeba project, 2024. Dataset hosted on Many-Things.org. 2

[33] Philipp Koehn. Europarl: A parallel corpus for statistical machine translation. In *Proceedings of machine translation summit x: papers*, pages 79–86, 2005. 3

[34] Rohit Kulkarni. Examine the examiner, 2021. Accessed: 2025-04-21. 2

[35] Xin Lai, Zhuotao Tian, Yukang Chen, Yanwei Li, Yuhui Yuan, Shu Liu, and Jiaya Jia. Lisa: Reasoning segmentation via large language model. 2024 IEEE/CVF Conference on Computer Vision and Pattern Recognition (CVPR), pages 9579–9589, 2023. 3, 4

[36] Yuhang Lan, Fei Shang, Jianhua Yang, Xiangui Kang, and Enping Li. Robust image steganography: hiding messages in frequency coefficients. In *Proceedings of the AAAI conference on artificial intelligence*, pages 14955–14963, 2023. 2, 6, 4, 7

[37] Chenliang Li, Haiyang Xu, Junfeng Tian, Wei Wang, Ming Yan, Bin Bi, Jiabo Ye, Hehong Chen, Guohai Xu, Zheng Cao, et al. mplug: Effective and efficient vision-language learning by cross-modal skip-connections. *arXiv preprint arXiv:2205.12005*, 2022. 2

[38] Junnan Li, Dongxu Li, Caiming Xiong, and Steven Hoi. Blip: Bootstrapping language-image pre-training for unified vision-language understanding and generation. In *International conference on machine learning*, pages 12888–12900. PMLR, 2022. 3

[39] Junnan Li, Dongxu Li, Silvio Savarese, and Steven Hoi. Blip-2: Bootstrapping language-image pre-training with frozen image encoders and large language models. In *International conference on machine learning*, pages 19730–19742. PMLR, 2023. 3

[40] Chin-Yew Lin. Rouge: A package for automatic evaluation of summaries. In *Text summarization branches out*, pages 74–81, 2004. 6

[41] Tsung-Yi Lin, Michael Maire, Serge Belongie, James Hays, Pietro Perona, Deva Ramanan, Piotr Dollár, and C Lawrence Zitnick. Microsoft coco: Common objects in context. In *Computer vision–ECCV 2014: 13th European conference, zurich, Switzerland, September 6–12, 2014, proceedings, part v 13*, pages 740–755. Springer, 2014. 6, 3

[42] Haotian Liu, Chunyuan Li, Qingyang Wu, and Yong Jae Lee. Visual instruction tuning. *Advances in neural information processing systems*, 36:34892–34916, 2023. 2, 3

[43] Haotian Liu, Chunyuan Li, Yuheng Li, and Yong Jae Lee. Improved baselines with visual instruction tuning. In *Proceedings of the IEEE/CVF Conference on Computer Vision and Pattern Recognition*, pages 26296–26306, 2024. 2

[44] Ilya Loshchilov and Frank Hutter. Decoupled weight decay regularization. *arXiv preprint arXiv:1711.05101*, 2017. 6

[45] Shao-Ping Lu, Rong Wang, Tao Zhong, and Paul L Rosin. Large-capacity image steganography based on invertible neural networks. In *Proceedings of the IEEE/CVF conference on computer vision and pattern recognition*, pages 10816–10825, 2021. 2

[46] Zheling Meng, Bo Peng, and Jing Dong. Latent watermark: Inject and detect watermarks in latent diffusion space. *IEEE Transactions on Multimedia*, 2025. 2

[47] Kishore Papineni, Salim Roukos, Todd Ward, and Wei-Jing Zhu. Bleu: a method for automatic evaluation of machine translation. In *Proceedings of the 40th annual meeting of the Association for Computational Linguistics*, pages 311–318, 2002. 6

[48] Hardik Patel and Preeti Dave. Steganography technique based on dct coefficients. *International Journal of Engineering Research and Applications*, 2(1):713–717, 2012. 2

[49] Lakshmi N. Pathi. Imdb dataset of 50k movie reviews, 2021. Dataset hosted on Kaggle. 2, 3

[50] Zhiliang Peng, Wenhui Wang, Li Dong, Yaru Hao, Shaohan Huang, Shuming Ma, Qixiang Ye, and Furu Wei. Grounding multimodal large language models to the world. In *The Twelfth International Conference on Learning Representations*, 2024. 4

[51] Fabien AP Petitcolas, Ross J Anderson, and Markus G Kuhn. Information hiding-a survey. *Proceedings of the IEEE*, 87(7):1062–1078, 2002. 11

[52] Aleksandar Petrov, Pierre Fernandez, Tomáš Souček, and Hady Elsahar. We can hide more bits: The unused watermarking capacity in theory and in practice. *arXiv preprint arXiv:2510.12812*, 2025. 6, 8, 9

[53] Taivo Pungas. A dataset of english plaintext jokes., 2017. 3

[54] Wenjie Qu, Wengui Zheng, Tianyang Tao, Dong Yin, Yanze Jiang, Zhihua Tian, Wei Zou, Jinyuan Jia, and Jiaheng Zhang. Provably robust multi-bit watermarking for {AI-generated} text. In *34th USENIX Security Symposium (USENIX Security 25)*, pages 201–220, 2025. 3

[55] Qwen, An Yang, Baosong Yang, Beichen Zhang, Binyuan Hui, Bo Zheng, Bowen Yu, Chengyuan Li, Dayiheng Liu, Fei Huang, Haoran Wei, Huan Lin, Jian Yang, Jianhong Tu, Jianwei Zhang, Jianxin Yang, Jiaxi Yang, Jingren Zhou, Junyang Lin, Kai Dang, Keming Lu, Keqin Bao, Kexin Yang, Le Yu, Mei Li, Mingfeng Xue, Pei Zhang, Qin Zhu, Rui Men, Runji Lin, Tianhao Li, Tianyi Tang, Tingyu Xia, Xingzhang Ren, Xuancheng Ren, Yang Fan, Yang Su, Yichang Zhang, Yu Wan, Yuqiong Liu, Zeyu Cui, Zhenru Zhang, and Zihan Qiu. Qwen2.5 technical report, 2025. 6, 3

[56] Abigail See, Peter J. Liu, and Christopher D. Manning. Get to the point: Summarization with pointer-generator networks. In *Proceedings of the 55th Annual Meeting of the Association for Computational Linguistics (Volume 1: Long Papers)*, pages 1073–1083, Vancouver, Canada, 2017. Association for Computational Linguistics. 1

[57] Abigail See, Peter J Liu, and Christopher D Manning. Get to the point: Summarization with pointer-generator networks. *arXiv preprint arXiv:1704.04368*, 2017. 3

[58] Kenneth Sullivan, Upamanyu Madhow, Shivkumar Chandrasekaran, and BS Manjunath. Steganalysis for markov

cover data with applications to images. *IEEE Transactions on Information Forensics and Security*, 1(2):275–287, 2006. 4

[59] Mitchell D Swanson, Mei Kobayashi, and Ahmed H Tewfik. Multimedia data-embedding and watermarking technologies. *Proceedings of the IEEE*, 86(6):1064–1087, 1998. 11

[60] Matthew Tancik, Ben Mildenhall, and Ren Ng. Stegastamp: Invisible hyperlinks in physical photographs. In *Proceedings of the IEEE/CVF conference on computer vision and pattern recognition*, pages 2117–2126, 2020. 1, 2, 4, 6, 7, 11

[61] Gemma Team, Aishwarya Kamath, Johan Ferret, Shreya Pathak, Nino Vieillard, Ramona Merhej, Sarah Perrin, Tatiana Matejovicova, Alexandre Ramé, Morgane Rivière, et al. Gemma 3 technical report. *arXiv preprint arXiv:2503.19786*, 2025. 6, 3

[62] Hugo Touvron, Thibaut Lavril, Gautier Izacard, Xavier Martinet, Marie-Anne Lachaux, Timothée Lacroix, Baptiste Rozière, Naman Goyal, Eric Hambro, Faisal Azhar, et al. Llama: Open and efficient foundation language models. *arXiv preprint arXiv:2302.13971*, 2023. 3

[63] Amalesh Vemula. Name and country of origin dataset, 2022. Dataset hosted on Kaggle. 1, 2

[64] Peng Wang, Shuai Bai, Sinan Tan, Shijie Wang, Zhihao Fan, Jinze Bai, Keqin Chen, Xuejing Liu, Jialin Wang, Wenbin Ge, Yang Fan, Kai Dang, Mengfei Du, Xuancheng Ren, Rui Men, Dayiheng Liu, Chang Zhou, Jingren Zhou, and Junyang Lin. Qwen2-vl: Enhancing vision-language model’s perception of the world at any resolution. *arXiv preprint arXiv:2409.12191*, 2024. 4

[65] Ran-Zan Wang, Chi-Fang Lin, and Ja-Chen Lin. Image hiding by optimal lsb substitution and genetic algorithm. *Pattern recognition*, 34(3):671–683, 2001. 2

[66] Yaofei Wang, Gang Pei, Kejiang Chen, Jinyang Ding, Chao Pan, Weilong Pang, Donghui Hu, and Weiming Zhang. Sparsamp: Efficient provably secure steganography based on sparse sampling. In *34th USENIX Security Symposium (USENIX Security 25)*, 2025. 3

[67] Jonathan J Webster and Chunyu Kit. Tokenization as the initial phase in nlp. In *COLING 1992 volume 4: The 14th international conference on computational linguistics*, 1992. 4

[68] Eric Wengrowski and Kristin Dana. Light field messaging with deep photographic steganography. In *Proceedings of the IEEE/CVF conference on computer vision and pattern recognition*, pages 1515–1524, 2019. 1, 2, 4, 7

[69] Jiarui Xu, Xingyi Zhou, Shen Yan, Xiuye Gu, Anurag Arnab, Chen Sun, Xiaolong Wang, and Cordelia Schmid. Pixel-aligned language model. In *Proceedings of the IEEE/CVF Conference on Computer Vision and Pattern Recognition*, pages 13030–13039, 2024. 3, 4

[70] Qinghao Ye, Haiyang Xu, Jiabo Ye, Ming Yan, Anwen Hu, Haowei Liu, Qi Qian, Ji Zhang, and Fei Huang. mplug-owl2: Revolutionizing multi-modal large language model with modality collaboration. In *Proceedings of the ieee/cvf conference on computer vision and pattern recognition*, pages 13040–13051, 2024. 2

[71] Weike You, Hong Zhang, and Xianfeng Zhao. A siamese cnn for image steganalysis. *IEEE Transactions on Information Forensics and Security*, 16:291–306, 2020. 6

[72] Jiwen Yu, Xuanyu Zhang, Youmin Xu, and Jian Zhang. Cross: Diffusion model makes controllable, robust and secure image steganography. *Advances in Neural Information Processing Systems*, 36:80730–80743, 2023. 1

[73] Chengsheng Yuan, Zhaonan Ji, Xinting Li, Zhili Zhou, Zhihua Xia, and QM Jonathan Wu. Dgadm-gis: Deterministic guided additive diffusion model for generative image steganography. *IEEE Transactions on Dependable and Secure Computing*, 2025. 2

[74] Yan Zeng, Xinsong Zhang, Hang Li, Jiawei Wang, Jipeng Zhang, and Wangchunshu Zhou. X<sup>2</sup>2-vlm: All-in-one pre-trained model for vision-language tasks. *IEEE Transactions on Pattern Analysis and Machine Intelligence*, 46(5):3156–3168, 2024. 4

[75] Chaoning Zhang, Philipp Benz, Adil Karjauv, Geng Sun, and In So Kweon. Udh: Universal deep hiding for steganography, watermarking, and light field messaging. *Advances in Neural Information Processing Systems*, 33:10223–10234, 2020. 4, 8

[76] Jingyi Zhang, Jiaxing Huang, Sheng Jin, and Shijian Lu. Vision-language models for vision tasks: A survey. *IEEE Transactions on Pattern Analysis and Machine Intelligence*, 2024. 2

[77] Tianyi Zhang, Varsha Kishore, Felix Wu, Kilian Q Weinberger, and Yoav Artzi. Bertscore: Evaluating text generation with bert. *arXiv preprint arXiv:1904.09675*, 2019. 6

[78] Xuanyu Zhang, Runyi Li, Jiwen Yu, Youmin Xu, Weiqi Li, and Jian Zhang. Editguard: Versatile image watermarking for tamper localization and copyright protection. In *Proceedings of the IEEE/CVF Conference on Computer Vision and Pattern Recognition (CVPR)*, pages 11964–11974, 2024. 1

[79] Xuanyu Zhang, Jiarui Meng, Runyi Li, Zhipei Xu, Yongbing Zhang, and Jian Zhang. Gs-hider: Hiding messages into 3d gaussian splatting. *Advances in Neural Information Processing Systems*, 37:49780–49805, 2024. 1

[80] Xiaorui Zhang, Rui Jiang, Wei Sun, and Sunil Kr Jha. Fppg: Increasing robustness of flow-based watermarking to unknown noise through feature preservation and gradient perturbation. *IEEE Transactions on Circuits and Systems for Video Technology*, 2025. 6, 4, 7

[81] Xuanyu Zhang, Zecheng Tang, Zhipei Xu, Runyi Li, Youmin Xu, Bin Chen, Feng Gao, and Jian Zhang. Omniduard: Hybrid manipulation localization via augmented versatile deep image watermarking. In *Proceedings of the Computer Vision and Pattern Recognition Conference*, pages 3008–3018, 2025. 1

[82] Boyang Zheng, Jinjin Gu, Shijun Li, and Chao Dong. Lm4lv: A frozen large language model for low-level vision tasks. *arXiv preprint arXiv:2405.15734*, 2024. 3

[83] Jiren Zhu, Russell Kaplan, Justin Johnson, and Li Fei-Fei. Hidden: Hiding data with deep networks. In *Proceedings of the European conference on computer vision (ECCV)*, pages 657–672, 2018. 2, 4, 8, 7

# S<sup>2</sup>LM: Towards Semantic Steganography via Large Language Models

## Supplementary Material

### Overview of the Supplementary Material

This supplementary document provides a comprehensive extension to the main paper, organized as follows:

- **Dataset Details (Sec. 7):** We introduce the proposed Invisible Text (IVT) benchmark, describe the construction of its three granular subsets (IVT-S/M/L), and provide detailed statistics on their text length, bit length, domains, and licenses. We also describe the construction of the LLM-generated IVT<sup>G</sup> dataset.
- **Experimental Details (Sec. 8):** We provide full training configurations for S<sup>2</sup>LM and baselines, including training dataset construction, model variants, optimization settings, implementation details, and retraining protocols for comparison methods.
- **Statistical Steganalysis (Sec. 9):** We conduct statistical steganalysis using StegExpose to evaluate the detectability of S<sup>2</sup>LM stego images and show that our method remains highly secure against classical statistical attacks.
- **Additional Experimental Results (Sec. 10):** We present comprehensive supplementary experiments, including using vision-language models within S<sup>2</sup>LM, constructing and benchmarking on the LLM-generated IVT<sup>G</sup> dataset, testing non-semantic messages, analyzing decoding with the original and cross-instance LLMs, applying 8-bit quantization on S<sup>2</sup>LM, and providing additional qualitative results.
- **Ablation Study Details (Sec. 11):** We visualize the spatial distribution of secret message embeddings under the mask strategy to analyze how it shapes SME layouts.
- **Analysis of Existing Methods (Sec. 12):** We analyze how existing UTF-based bitstream representations and MLP designs inherently constrain capacity and scalability of current steganographic methods.
- **Discussion (Sec. 13):** We discuss the motivation behind semantic steganography, as well as the broader impacts, potential risks, and mitigation strategies associated with S<sup>2</sup>LM.
- **Background and Preliminaries (Sec. 14):** We clarify the terminology and related notions, such as the cover image and the stego image, used throughout this work.

### 7. Invisible Text Dataset

To evaluate the effectiveness of semantic steganography, we construct a new benchmark dataset named **InVisible Text** (IVT). IVT is a large-scale dataset specifically designed for semantic steganography research, where the secret information consists of natural language text with varying degrees of complexity and length.

Specifically, we collect text information from various open-source datasets, including Translation, Question Answering, Sentiment Analysis, and Information Extraction *et al.* To facilitate systematic evaluation and controlled experimentation, we divide IVT into three subsets of increasing granularity: IVT-S, IVT-M, and IVT-L. These subsets differ in the length, structure, and semantic richness of the secret messages:

- IVT-S contains short phrases or word-level content targeting lightweight steganography scenarios.
- IVT-M contains complete sentences or short sentence pairs, balancing semantic richness and embedding complexity.
- IVT-L contains full natural-language paragraphs, serving as a high-capacity and semantically dense benchmark.

The word length distribution of IVT is shown in Figure 7. This three-granularity design enables comprehensive performance analysis across varying semantic loads, offering insights into the scalability, robustness, and text fidelity of semantic steganographic frameworks.

#### 7.1. IVT-S

IVT-S is the simplest variant in IVT, focusing on short, low-capacity messages. Each secret message in IVT-S consists of a short phrase or a few words, typically ranging from 5 to 20 words. This setting reflects minimal semantic load, making it suitable for testing basic sentence-level embedding capabilities. IVT-S serves as a lightweight benchmark for evaluating models under low-information embedding scenarios.

The IVT-S dataset covers a wide range of short textual types, including real person names [63], news headlines [3], paper titles [16], Twitter comments [20], and dialogue snippets [1]. For more details on IVT-S, please refer to Table 4.

#### 7.2. IVT-M

IVT-M is a medium-granularity subset in IVT, positioned between the short messages of IVT-S and the full-paragraph texts of IVT-L. Each secret message in IVT-M consists of coherent sentences with a length of about 50 to 100 words. This setting introduces moderate semantic complexity and content richness, making it ideal for evaluating models under typical sentence-level steganography scenarios. IVT-M reflects more realistic use cases than IVT-S by requiring the model to encode and recover messages with non-trivial structure and meaning.

Messages in IVT-M are sourced from a variety of domains, including CNN news abstracts [56], Wikipedia sum-

Table 4. The composition of the IVT-S.

Category	Source	Bit Length			Word Length			Unique Word	Sample Number	License
		Average	Max	Min	Average	Max	Min			
Paper title	arxiv-10 [16]	592.2	1296	120	9.7	20	2	4576	1000	GPL-3.0
News title	PENS [3]	506.9	1072	120	10.3	20	2	5506	1000	MSR License
Article title	examiner [34]	423.1	800	40	8.6	19	1	4873	1000	CC0 1.0 License
People name	name&code [63]	113.8	200	72	2.1	4	2	857	1000	-
Sentence	cnn-en [32]	247.3	848	40	6.2	18	1	1946	1000	CC-BY 2.0 License
Dialogue	SP-S1 [1]	202.9	520	32	4.5	9	1	1924	1000	-
Comment	sentiment140 [20]	486.2	1120	56	10.7	20	1	4374	1000	-
Overall	-	367.5	836.6	68.6	7.4	15.7	1.4	19941	7000	-

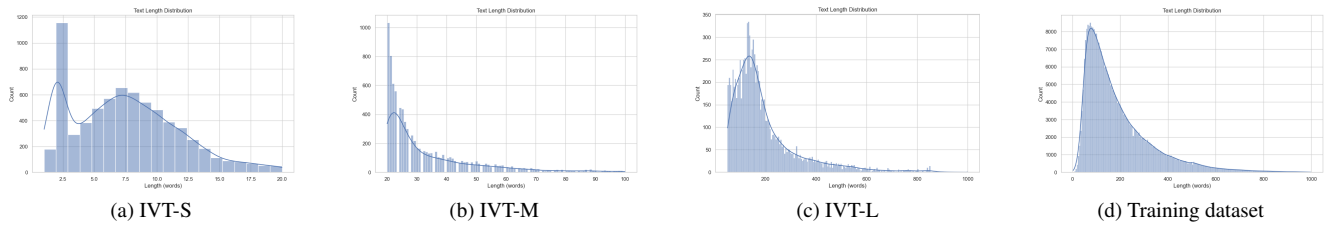


Figure 7. Word length distribution in IVT and training dataset.

maries [18], IMDB reviews [49]. For more details about IVT-M, please refer to Table 5.

### 7.3. IVT-L

IVT-L represents the largest and most challenging subset of the IVT dataset, designed to evaluate a model’s ability to embed and recover long-form semantic content. Each secret message in IVT-L consists of a full paragraph containing multiple sentences with coherent structure, complex syntax, and a diverse vocabulary, with a length of about 100 to 500 words. Compared to IVT-S and IVT-M, IVT-L significantly enhances the semantic richness and information density of the hidden text, thereby imposing greater demands on a model’s capacity, fidelity, and ability to preserve semantics. This subset serves as a benchmark for evaluating whether steganographic models can scale to real-world scenarios that involve concealing full-length, meaningful textual content.

IVT-L includes long-form messages drawn from a variety of sources, including narrative news passages, short stories [15, 22], research paper abstracts [16], IMDB reviews [49]. These samples span multiple domains and writing styles, providing a comprehensive benchmark for evaluating sentence-to-image steganography in high-capacity settings. For more details about IVT-L, please refer to Table 6.

### 7.4. IVT<sup>G</sup>

To further assess the ability of our S<sup>2</sup>LM, we construct a new dataset named IVT<sup>G</sup>, which is entirely synthesized

by the LLM. Specifically, we leverage the DeepSeek [14] API to generate the textual content. Similar to the original IVT dataset, we divide IVT<sup>G</sup> into three subsets based on the length of the secret text.

## 8. Experimental Details

To explore the feasibility and performance of sentence-to-image steganography powered by large language models, we propose three variants of our framework, namely S<sup>2</sup>LM-Qwen2.5-0.5B, S<sup>2</sup>LM-Llama3.2-1B, and S<sup>2</sup>LM-MiniCPM-1B. These models are built upon different backbone LLMs with varying scales and capabilities, providing diverse perspectives on model behavior across capacity and architecture. In the following sections, we detail the training procedures and dataset construction strategies used for each model, including how the secret messages are formatted, encoded, and paired with cover images to form effective training samples. This enables a thorough evaluation of how different LLMs perform under the semantic steganography task. For all baseline methods, we follow the training settings described in their original papers to ensure a fair comparison.

### 8.1. Training Dataset of S<sup>2</sup>LM

**Text Dataset.** We use the English subset of the WanJuan [25] Text Dataset as our text dataset. WanJuan 1.0 Text Dataset is composed of cleaned pre-training corpora from different sources such as web pages, encyclopedias, books, patents, textbooks, and exam questions. The total amount of data exceeds 500 million documents, and the data size

Table 5. The composition of the IVT-M.

Category	Source	Bit Length			Word Length			Unique Word	Sample Number	License
		Average	Max	Min	Average	Max	Min			
Paper title	arxiv-10 [16] PENS [3] CNN and Daily mail [57] WMT-14 [7] stupid joke [53] europarl [33] South Park [1] hate text [13] moral story [22]	1210.0	1904	696	22.0	38	20	7776	1000	GPL-3.0
New title		1369.4	1968	624	23.0	41	20	8003	1000	MSR License
News highlight		2303.6	4896	736	50.3	100	20	13119	1000	Apache 2.0
Translate text		1610.1	4776	672	33.8	98	20	6760	1000	-
Joke story		2042.1	17648	592	47.6	100	20	10637	1000	-
Translate text		1618.8	5344	744	34.0	99	20	6735	1000	-
Dialogue		1367.1	4040	688	31.7	92	20	3896	1000	-
Comment		989.9	1120	552	23.4	33	20	6564	1000	MIT License
Moral		1369.4	4728	680	32.5	97	20	3179	1000	CC BY-NC-SA 3.0
Overall	-	1542.3	17648	552	33.1	100	20	49423	9000	-

Table 6. The composition of the IVT-L.

Category	Source	Bit Length			Word Length			Unique Word	Sample Number	License
		Average	Max	Min	Average	Max	Min			
Paper abstract	arxiv-10 [16] wiki [18] stupid joke [53] moral story [22] Tiny Story [15] IMDB [49] yelp [4] asap-aes [17]	8589.8	15360	2424	157.8	325	50	22705	1000	GPL-3.0
Wiki abstract		7840.5	40776	2216	157.5	863	50	26582	1000	GFDL/CC BY-SA
Story		7285.7	41168	1920	166.4	997	50	25232	1000	-
Story		11374.1	42576	1920	265.0	956	50	20898	1000	-
Story		6957.5	33192	2600	166.4	813	64	10348	1000	-
User review		10457.4	45736	2048	231.0	1000	50	34259	1000	IMDB License
User review		5996.6	39664	1968	138.9	871	50	18029	1000	Yelp License
Composition		10435.9	39216	1912	238.5	897	50	17289	1000	-
Overall	-	8675.3	45736	1912	194.5	1000	50	118472	8000	-

exceeds 1TB. We selected a subset of the English dataset (4 GB). For texts that spanned multiple lines, we removed “\n”, “\s” and extra spaces to merge them into single lines. We then extracted texts with fewer than 1,000 words, resulting in 3,537,390 samples. Finally, we randomly selected 320,000 samples to construct the training set. The distribution of text lengths in the training set is shown in Fig. 7.

**Image Dataset.** We use the COCO Training Dataset [41] training dataset as our cover image dataset.

## 8.2. Implementation Details

**LoRA Config.** We employ Low-Rank Adaptation (LoRA) with a rank  $r = 8$  to fine-tune the pretrained LLM using the peft library, injecting trainable low-rank matrices into the query and key projection layers (q\\_proj, k\\_proj). The LoRA scaling factor  $\alpha$  is set to 32 with a dropout rate of 0.1.

**Trainer.** We train the model using the Trainer of the transformers library. The S<sup>2</sup>LM is optimized via the AdamW optimizer with a learning rate of 2e-4 and weight decay of 0.01 for regularization. The learning rate follows a cosine scheduler with 500 warmup steps to stabilize early training. We use mixed-precision training to accelerate convergence while maintaining numerical stability. The two-stage training shares the same config.

**Computation Platform.** All experiments are conducted on NVIDIA A800 80GB GPUs with CUDA Version 12.4.

**S<sup>2</sup>LM-Qwen2.5-0.5B.** S<sup>2</sup>LM-Qwen2.5-0.5B is built upon the Qwen2.5-0.5B backbone [55] and fine-tuned using the LoRA config mentioned above. The training strategy is detailed in Section 4.3. In Stage 1, we use a batch size of 14 and train for one epoch. In Stage 2, we train for 6,000 iterations with a batch size of 14.

**S<sup>2</sup>LM-Llama3.2-1B.** S<sup>2</sup>LM-Llama3.2-1B is built upon the Llama3.2-1B backbone [21] and fine-tuned using the LoRA config mentioned above. The training strategy is detailed in Section 4.3. In Stage 1, we use a batch size of 14 and train for one epoch. In Stage 2, we train for 6,000 iterations with a batch size of 14.

**S<sup>2</sup>LM-MiniCPM-1B.** S<sup>2</sup>LM-MiniCPM-1B is built upon the MiniCPM-1B backbone [28] and fine-tuned using the LoRA config mentioned above. The training strategy is detailed in Section 4.3. In Stage 1, we use a batch size of 24 and train for one epoch. In Stage 2, we train for 5,000 iterations with a batch size of 24.

**S<sup>2</sup>LM-Gemma3-1B.** S<sup>2</sup>LM-Gemma3-1B is built upon the Gemma3-1B backbone [61] and fine-tuned using the LoRA config mentioned above. The training strategy is detailed in Section 4.3. In Stage 1, we use a batch size of 14 and train

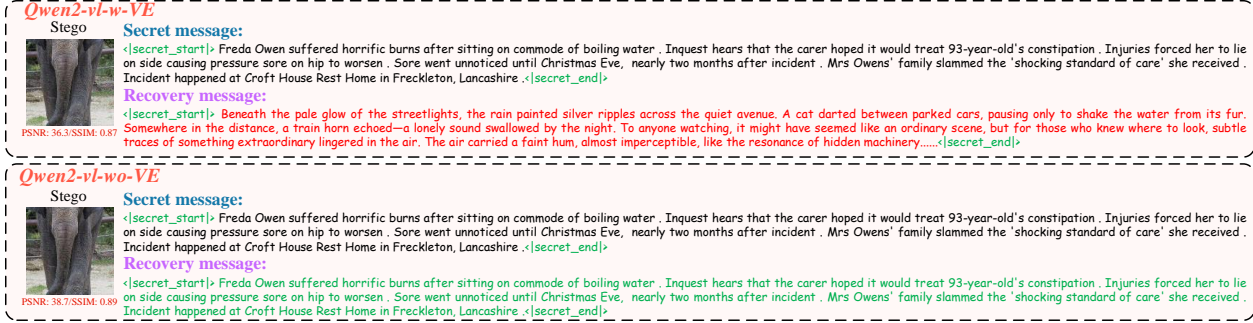


Figure 8. a failure case of  $S^2LM$ -Qwen2-vl-2B on IVT-L. The model can output the `(SECRET_START)` and `(SECRET_END)` tokens. However, the recovered text is entirely different from the ground-truth message.

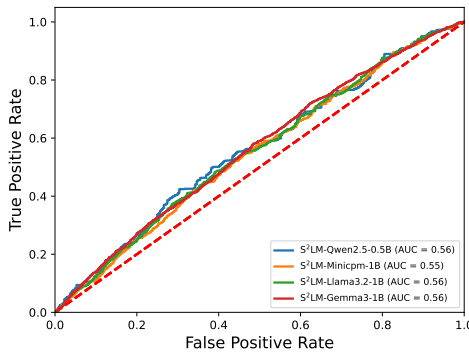


Figure 9. The ROC curve produced by StegExpose for  $S^2LM$ .

for one epoch. In Stage 2, we train for 6,000 iterations with a batch size of 14.

**StegaStamp.** We retrain StegaStamp [60] with extended capacity (from 100 bits to 512 bits) on cover images with  $256 \times 256$  resolution using the Flickr2K dataset. The model is optimized with AdamW with learning rate set to  $2e-4$  for 15,000 iterations with batch size set to 16. While achieving stable convergence, we observe fundamental limitations: the 512-bit encoding yields only  $\sim 70\%$  bit accuracy, resulting terrible performance in IVT. This suggests current spatial-domain watermarking architectures struggle with high-capacity payloads with primitive representation of secret message such as UTF codes. More details can be found in Sec. 12.2.

**LanNet.** We retrain LanNet [36] on cover images with  $256 \times 256$  resolution using the DIV2K training dataset. The model is optimized with AdamW with learning rate set to  $2e-4$  for 1,000 epochs with batch size set to 12.

**FPGP.** We retrain FPGP [80] on cover images with  $256 \times 256$  resolution using the DIV2K training dataset. The model is optimized with AdamW with learning rate set to  $2e-4$  for 1,000 epochs with batch size set to 12.

**CRMark.** We retrain CRMark [10] on cover images with

Table 7. K-L divergence between cover images and stego images produced by different methods.  $S^2LM$ -Q denotes  $S^2LM$ -Qwen2.5-0.5B.

Methods	$S^2LM$ -Q	DwtDet	StegaStamp	LanNet	FPGP	CRMark
K-L	0.0015	0.082	0.072	0.0024	0.0017	0.0019

$256 \times 256$  resolution using the DIV2K training dataset. The model is optimized with AdamW with learning rate set to  $1e-4$  for 1000 epochs with batch size set to 12.

## 9. Statistical Steganalysis

We use StegExpose [6] to measure the  $S^2LM$  anti-steganalysis ability. The receiver operating characteristic (ROC) curve in Figure 9 shows that  $S^2LM$  has high security and can fool the StegExpose.

K-L divergence provides a convenient means of gauging how easy it is to discriminate between cover and stego. Typical cover data, however, are not i.i.d. (independent and identically distributed). For example, both pixels and audio samples are known to be highly correlated [58]. Therefore, KL divergence is insufficient as a standalone criterion for evaluating steganographic security [58]. Nevertheless, we compute the K-L divergence between the stego images generated by  $S^2LM$  and the original cover images. As shown in Tab. 7, all steganographic models achieve very small KL divergence values, with  $S^2LM$  getting the best result.

## 10. Supplementary Experiments

### 10.1. VLMs in $S^2LM$

In the previous experiments, all models were based on pure text-only large language models. To further explore the applicability of vision-language models (VLMs) to the sentence-to-image steganography task, we conducted additional experiments using Qwen2-vl [64] as a representative VLM. However, the results showed that Qwen2-vl failed to fit the training data. Fig. 8 shows a failure case of

Table 8. Quantitative results on the IVT<sup>G</sup>-S, IVT<sup>G</sup>-M, and IVT<sup>G</sup>-L benchmarks.

Methods	IVT <sup>G</sup> -S								IVT <sup>G</sup> -M								IVT <sup>G</sup> -L							
	Secret/Recovery				Cover/Stego				Secret/Recovery				Cover/Stego				Secret/Recovery				Cover/Stego			
	WER	BLEU	ROUGE	BERT-S	PSNR	SSIM	WER	BLEU	ROUGE	BERT-S	PSNR	SSIM	WER	BLEU	ROUGE	BERT-S	PSNR	SSIM	WER	BLEU	ROUGE	BERT-S	PSNR	SSIM
S <sup>2</sup> LMQwen2.5-0.5B	0.040	0.911	0.944	0.953	41.6	0.960	0.034	0.933	0.963	0.966	39.1	0.984	0.047	0.916	0.959	0.958	40.2	0.968						
S <sup>2</sup> LMMiniCPM-1B	0.040	<b>0.935</b>	<b>0.972</b>	<b>0.977</b>	42.4	0.988	0.040	<b>0.939</b>	<b>0.973</b>	<b>0.976</b>	42.5	0.987	0.054	<b>0.919</b>	<b>0.963</b>	<b>0.963</b>	42.8	0.984						
S <sup>2</sup> LMLlama3.2-1B	<b>0.037</b>	0.916	0.947	0.961	<b>45.6</b>	<b>0.991</b>	<b>0.039</b>	0.887	0.920	0.938	<b>46.6</b>	<b>0.989</b>	<b>0.040</b>	0.739	0.804	0.844	<b>43.1</b>	<b>0.988</b>						
S <sup>2</sup> LMGemma3-1B	0.067	0.767	0.819	0.866	43.5	0.980	0.096	0.730	0.797	0.852	43.6	0.977	0.157	0.726	0.815	0.866	39.2	0.932						

Table 9. Quantitative results of S<sup>2</sup>LM-Qwen2-vl-2B on IVT-L. Qwen2-vl fails to decode the hidden message with vision encoder (S<sup>2</sup>LM-Qwen2-vl-w\_VE). When the vision encoder is removed, Qwen2-vl works well (S<sup>2</sup>LM-Qwen2-vl-wo\_VE). This contrast highlights the gap between visual understanding and image steganography: the original visual encoder may in fact hinder Qwen2-vl’s ability to capture low-level steganographic signals.

Methods	WER	BLEU-4	ROUGE	BERT-S	PSNR		SSIM
					PSNR	SSIM	
S <sup>2</sup> LM-Qwen2-vl-wo_VE	0.982	0.012	0.035	0.106	33.51	0.827	
S <sup>2</sup> LM-Qwen2-vl-w_VE	0.152	0.841	0.832	0.890	32.16	0.812	

Table 10. Quantitative result on the IVT-L benchmark of 8-bit quantized S<sup>2</sup>LM-Qwen2.5-0.5B.

Methods	WER	BLEU-4	ROUGE	BERT-S	PSNR		SSIM
					PSNR	SSIM	
S <sup>2</sup> LM-Qwen2.5-0.5B-8bit	0.201	0.804	0.882	0.907	40.05	0.946	

S<sup>2</sup>LM-Qwen2-vl-2B on IVT-L. The model can output the ⟨SECRET\\_START⟩ and ⟨SECRET\\_END⟩ tokens. However, the recovered text is entirely different from the ground-truth message.

We hypothesize that this underperformance stems from the **fundamental difference between visual understanding and steganography**. While VLMs are primarily optimized for visual tasks, which focusing on understanding objects, scenes, and spatial relationships within images. However, steganography emphasizes decoding secret messages by focusing on imperceptible signals embedded within images. Unlike typical vision-language alignment tasks, steganography does not require high-level visual semantics but rather the capacity to detect and interpret fine-grained patterns that are deliberately encoded. This highlights the need for models specifically tailored to the semantic embedding and recovery processes intrinsic to image-based steganography.

To validate our hypothesis, we conducted an ablation study by removing the visual encoder of Qwen2-vl. As shown in Tab. 9, under this setting, the Qwen2-vl works well on IVT-L, suggesting that its original visual encoder may in fact hinder its ability to capture low-level steganographic signals.

## 10.2. Model Quantization

We use a lightweight language model ( $\leq 1B$ ), which runs efficiently on edge devices such as mobile phones. After applying 8-bit quantization, its memory usage of the S<sup>2</sup>LM-Qwen2.5-0.5B is **below 200 MB**, making the entire framework both practical and scalable. As shown in the table below, the 8-bit quantized version of S<sup>2</sup>LM-Qwen2.5-0.5B processes the IVT-L dataset effectively **without any quantization-aware training**, with GPU memory usage of **less than 2 GB** during inference.

## 10.3. Experiments on Generative Message

To further assess the ability of our S<sup>2</sup>LM, we construct a new dataset named IVT<sup>G</sup>, which is entirely synthesized by the LLM. Specifically, we leverage the DeepSeek [14] API to generate the textual content. Similar to the original IVT dataset, we divide IVT<sup>G</sup> into three subsets based on the length of the secret text.

As shown in Table 8, our model S<sup>2</sup>LM achieves comparable performance on IVT<sup>G</sup> to its performance on the original IVT dataset. This consistency demonstrates the model’s ability to generalize to data generated by large language models, further validating the effectiveness of our approach.

## 10.4. Experiments on Non-semantic Message

Under the definition of semantic steganography, secret messages are assumed to be natural language information. All of our experiments follow this assumption. However, not all text carries semantic content. For instance, a random character string or a sequence of bits conveys no meaningful information, and transmitting such data offers limited practical utility. Nevertheless, some forms of non-semantic text do appear in real-world scenarios, such as URLs or cryptographic keys. To evaluate these cases, we tested S<sup>2</sup>LM on several representative examples and visualized the results. As shown in Fig. 10, S<sup>2</sup>LM-Qwen2.5-0.5B **maintains strong performance even in these settings**.

## 10.5. Decoding with the Original LLM

We evaluate the security of S<sup>2</sup>LM under a stronger and more practical adversarial assumption: the adversary successfully identifies the exact LLM used in our framework.



Figure 10. Qualitative results of  $S^2LM$  on no-semantic information.

Table 11. Decoding results on IVT-L using original Qwen2.5-0.5B and different Qwen2.5-0.5B.

Methods	WER	BLEU-4	ROUGE	BERT-S
Original Qwen2.5-0.5B	1.000	0.000	0.003	0.336
Different Qwen2.5-0.5B	1.000	0.000	0.004	0.324

Specifically, we conduct experiments on  $S^2LM$ -Qwen2.5-0.5B and assume that the adversary knows the concrete LLM and has even obtained the Patch-to-Token MLP  $\mathcal{F}_{P2T}$ . In this setting, we generate stego images using the fine-tuned Qwen2.5-0.5B, while the adversary attempts to decode the hidden messages using the original Qwen2.5-0.5B. All prompts and decoding configurations remain unchanged.

As illustrated in Tab. 11 (Original Qwen2.5-0.5B), the decoding results are extremely poor: the recovered text contains little to no semantic correspondence to the ground truth. This observation confirms that, even when the adversary correctly identifies the underlying LLM and gains access to  $\mathcal{F}_{P2T}$ , the hidden information cannot be decoded without the fine-tuned decoding alignment.

In conclusion,  $S^2LM$  remains secure under this strong known-model assumption if the weight of the LLM is not leaked.

## 10.6. Decoding Using Cross-Instance LLM

We further assess the security of  $S^2LM$  by examining whether independently trained model instances are mutually decodable. Using identical training configurations but different random seeds, we obtain two variants of  $S^2LM$ -Qwen2.5-0.5B, denoted as  $S^2LM$ -A and  $S^2LM$ -B. In this experiment, we use  $S^2LM$ -A to generate stego image, while  $S^2LM$ -B is used for decoding information from stego image.

Despite sharing the same architecture, training hyper-parameters, and optimization procedure,  $S^2LM$ -B fails to recover meaningful messages from stego images generated by  $S^2LM$ -A, as shown in the Tab. 11 (Different Qwen2.5-0.5B). These findings indicate that the steganographic latent

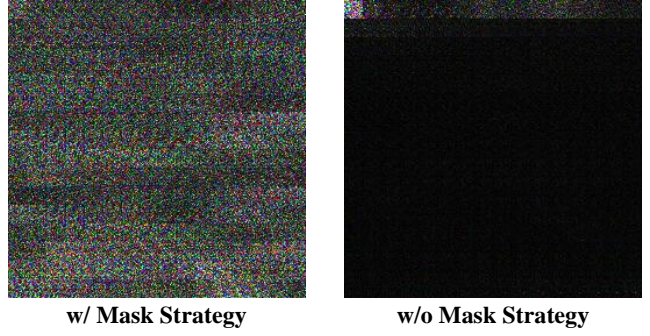


Figure 11. The Visualization of SMEs w/ or w/o mask strategy, which are enhanced by 5x for better visualization.

alignment learned during fine-tuning is instance-specific and not transferable across independently trained models, further demonstrating the robustness of  $S^2LM$  to cross-instance decoding attempts.

## 11. More Details about Ablation Study

### 11.1. Impact of Mask Strategy

In decoding process of the first stage, we mask some input tokens to encourage LLM distribute the information in the whole cover image. As shown in Figure 11, the SMEs are evenly distributed after training with the mask strategy, and significant improvements in recovery quality are observed in Table 3.

## 12. Analysis of Existing Methods

### 12.1. Choice of the Baselines

To ensure a fair and reasonable comparison, we select several representative methods from the field of image steganography as our baselines. Our chosen baselines include both traditional methods (DwtDct) and deep learning-based models (StegaStamp, LanNet, FPGP, CRMark). In the original paper of StegaStamp, the authors categorize their method as steganography. However, following the terminology adopted in prior literature, we classify it as a wa-

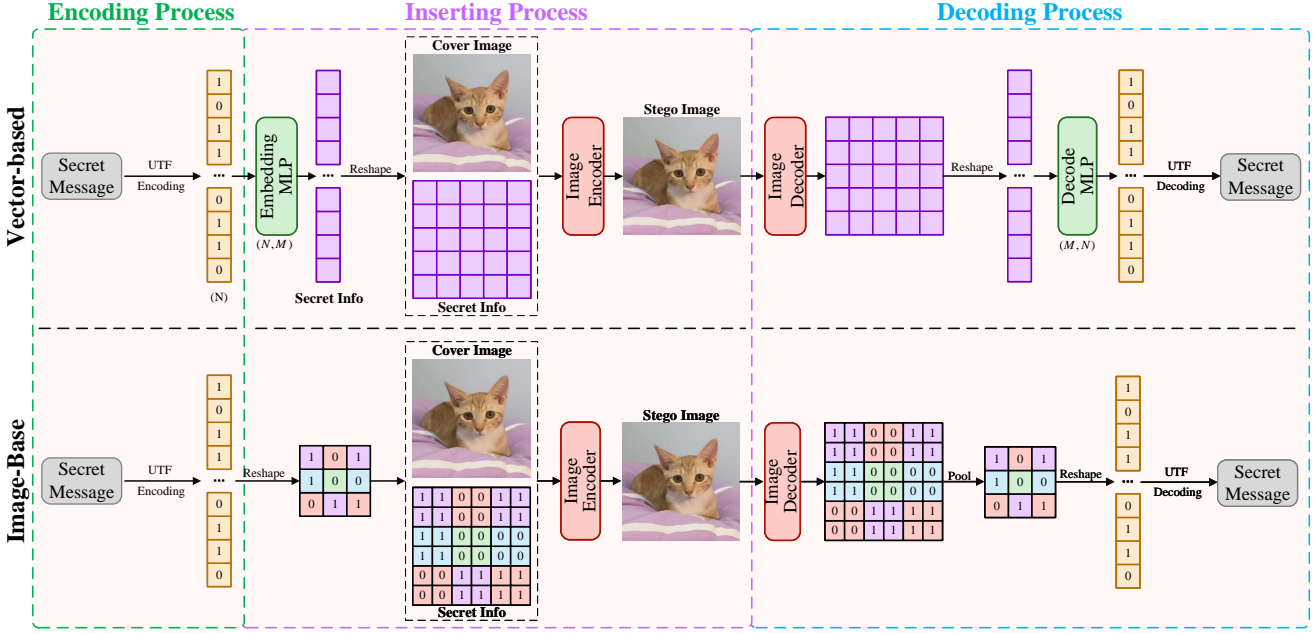


Figure 12. The architectural details of existing method. Existing models can be categorized into vector-based and image-based methods according to how they process the secret message.

termarking method, as it takes robustness into considerations. However, in our experiments, **we remove the robustness constraint to align them with the definition of steganography**. All deep learning-based baselines are re-trained for a fair comparison.

## 12.2. Why Existing Model Fail?

As illustrated in the Fig. 12, we show the architectural details of existing methods. To facilitate further analysis, we categorize existing models into two types based on how they process the secret message: **vector-base models** [60, 68, 83] and **image-based models** [10, 36, 80]. Vector-based methods employ MLPs to transform bitstreams into vector representation. During the embedding process, an embedding MLP first converts the bit sequence into a latent vector, which is then reshaped to match the spatial resolution of the cover image. This latent representation is subsequently fused with the cover image through an image encoder to produce the stego image. For message recovery, the stego image is processed by an image decoder to extract feature maps, which are flattened and passed through a decoding MLP to reconstruct the original binary message. In contrast, image-based methods omit the use of MLPs. Instead, the raw bit sequence is directly reshaped into a two-dimensional (2D) map and up-sampled (up-sample is optional) to align with the resolution of cover image. Then, the 2D representation of bitstreams will concat with cover image to produce stego image by image encoder. The stego image is then decoded by an image decoder to recover the

2D secret map, which is average pooled (pooling is optional) and flattened to reconstruct the final message. All of these two types of approaches encode textual information into bitstreams using UTF encoding for embedding and extraction. While this design is straightforward, it fails to preserve the semantic characteristics of the original text.

In our experiments reported in the main paper, we found that existing models exhibit a notable limitation in steganographic capacity. Although some of these methods were originally evaluated under watermarking task settings, where a trade-off between robustness and capacity is necessary, our additional experiments in Sec. 12.4 suggest that **robustness is not the primary factor causing this limitation. Instead, the architectural design fundamentally constrains the upper bound of steganographic capability**. This structural limitation has been largely overlooked in previous studies, overshadowed by concerns about robustness. In summary, existing methods face two main limitations, as described below.

**Limitations of Binary Representation.** Existing methods typically employ UTF-based encoding for secret messages. Specifically, the textual content is first converted into a binary sequence through UTF encoding and then processed by subsequent modules. However, this binary representation introduces several inherent limitations.

**(1) Low information density.** UTF encoding is a manually designed one-to-one mapping that lacks linguistic structures such as words, morphemes, or syntax. Consequently, it provides no inductive bias, hindering the model’s

ability to learn meaningful representations in subsequent procedures.

**(2) Excessive sequence length.** The UTF encoding scheme represents each character with 8 bits, leading to excessively long binary sequences that are inefficient and cumbersome to process.

**(3) Limited capacity and scalability.** Both types of methods require reshaping the binary sequence to align with the spatial resolution of the image. Consequently, a maximum bit length must be predefined: shorter sequences are padded, whereas longer ones are truncated. As illustrated in Fig. 12, in vector-based methods using an MLP, both the input dimension  $N$  and output dimension  $M$  are fixed. Similarly, in image-based methods where the binary sequence is directly concatenated with image features, the reshaped sequence must match the pixel resolution. Therefore, existing models can only process fixed-length bit sequences, it is a rigid constraint that also imposes a fixed resolution on the cover image.

**Limitations of MLP.** Once the secret message is converted into a binary sequence, it is typically processed by a multi-layer perceptron (MLP) to obtain a latent representation. However, this operation introduces several critical issues:

**(1) Poor generalization.** As a fully connected network, the MLP lacks the ability to capture local or global dependencies within the input sequence. Moreover, binary encoding is inherently structureless, which severely reduces representational efficiency. Since UTF-based binary representations carry no linguistic inductive bias, the MLP struggles to learn meaningful or generalizable patterns.

**(2) Limited capacity and flexibility.** Because the MLP’s input and output dimensions are fixed, it can only handle binary sequences of a specific length. This rigid design constrains the model’s capacity and prevents it from adapting to messages of variable length.

**(3) Parameter explosion.** When the binary sequence is long, the MLP must process extremely high-dimensional inputs. For example, with an input length of 4,096 bits and a hidden dimension of 512, the first layer alone contains more than two million parameters, rendering the model inefficient to train.

To validate our conclusion that the architectural design of existing methods fundamentally limits the capabilities of current steganographic techniques, we conduct comprehensive experiments in the following section. The results indicate that the observed capacity bottleneck stems from the model architecture rather than from robustness considerations.

**Inverse Wooden Barrel Effect.** Traditional steganographic models are typically trained for a fixed maximum message capacity. Under this setting, the model must accommodate the longest possible message, even though real-world communications rarely reach this limit. As a result, the architec-

Table 12. Capacity analysis of StegaStamp. StegaStamp maintains stable decoding at low payloads but degrades sharply at 512 bits. At 1024 bits, StegaStamp collapses and fails to recover any information.

Capacity	PSNR	SSIM	Bit Accuracy	Byte Accuracy
256 bit	45.91	0.9792	1.0000	1.0000
512 bit	43.40	0.9568	0.7597	0.0553
768 bit	40.48	0.9103	0.6910	0.0222
1024 bit	50.12	0.9999	0.5039	0.0021

Table 13. Capacity analysis of CRMark. CRMark collapses at a payload of 0.25 bpp, where both decoding and visual quality degrade may due to the inherent invertibility of the INN architecture.

Capacity	PSNR	SSIM	Bit Accuracy	Byte Accuracy
0.015 bpp (1024 bits)	45.92	0.9892	1.0000	1.0000
0.0625 bpp (4096 bits)	37.02	0.9201	1.0000	1.0000
0.25 bpp (16384 bits)	30.10	0.8115	0.5516	0.0035
1 bpp (65536 bits)	25.18	0.6602	0.5208	0.0038

ture is forced to scale its internal capacity, like constructing a barrel tall enough to hold the deepest possible fill. In practice, however, only a small portion of this capacity is used, leaving most of it wasted.

We term this mismatch the Inverse Barrel Effect. In contrast to the classical barrel effect, where the shortest stave limits the total volume, here the longest stave determines the overall design. The model must be overparameterized to satisfy the largest capacity requirement, resulting in redundant computation, and potentially degraded performance when embedding short messages.

### 12.3. Capacity Analysis of Existing Models.

To validate the above analysis, we evaluated the capacity limits of existing models after removing robustness constraints. We selected two representative methods, StegaStamp (vector-based method) and CRMark (image-based method). For StegaStamp, we expanded its capacity by adjusting the embedding MLP to support 256, 512, 768, and 1024 bits. For CRMark, we tested the model under different payload rates of 0.015625, 0.0625, 0.25, and 1 bits per pixel (bpp). The resolution of cover image is fixed to  $256 \times 256$ .

Our findings are consistent with recent results reported by Meta [52]. For StegaStamp, when the capacity is increased to 1024 bits, the model exhibits clear mode collapse: the decoder fails to recover any meaningful secret information, and the encoder also stops functioning properly. Similarly, for CRMark, its decoding performance degrades substantially when the payload reaches 0.25 bpp. Notably, this decrease in decoding accuracy is accompanied by a de-

Table 14. Robustness evaluation on the IVT dataset under different attack settings.  $S^2LM\text{-Q}$  denotes  $S^2LM\text{-Qwen2.5-0.5B}$ . Across all attack scenarios,  $S^2LM$  maintains consistently high decoding accuracy, while baseline methods suffer substantial performance drops.

Attack	Methods	IVT-S								IVT-M								IVT-L								
		Secret/Recovery				Cover/Stego		Secret/Recovery				Cover/Stego		Secret/Recovery				Cover/Stego								
		WER	BLEU	ROUGE	BERT-S	PSNR	SSIM	WER	BLEU	ROUGE	BERT-S	PSNR	SSIM	WER	BLEU	ROUGE	BERT-S	PSNR	SSIM	WER	BLEU	ROUGE	BERT-S	PSNR	SSIM	
Gaussian Blur	StegaStamp	0.402	0.231	0.125	0.332	-	-	-	-	-	-	-	-	-	-	-	-	-	-	-	-	-	-	-	-	
	DwtDet	1.000	0.000	0.000	0.292	-	-	-	-	-	-	-	-	-	-	-	-	-	-	-	-	-	-	-	-	
	FPGP	0.134	0.602	0.935	0.922	-	-	0.821	0.485	0.565	0.491	-	-	-	-	-	-	-	-	-	-	-	-	-	-	
	LanNet	0.010	0.783	0.927	0.989	-	-	0.251	0.682	0.782	0.815	-	-	0.910	0.056	0.142	0.382	-	-	-	-	-	-	-	-	
	CRMark	0.012	0.735	0.952	0.962	-	-	0.173	0.752	0.802	0.863	-	-	0.859	0.102	0.147	0.420	-	-	-	-	-	-	-	-	
	$S^2LM\text{-Q}$	0.042	0.842	0.883	0.965	-	-	0.042	0.961	0.978	0.975	-	-	0.081	0.912	0.972	0.965	-	-	-	-	-	-	-	-	
Brightness	StegaStamp	0.443	0.252	0.251	0.389	-	-	-	-	-	-	-	-	-	-	-	-	-	-	-	-	-	-	-	-	
	DwtDet	1.000	0.000	0.000	0.304	-	-	-	-	-	-	-	-	-	-	-	-	-	-	-	-	-	-	-	-	
	FPGP	0.141	0.721	0.893	0.904	-	-	0.747	0.434	0.552	0.454	-	-	-	-	-	-	-	-	-	-	-	-	-	-	
	LanNet	0.031	0.715	0.982	0.927	-	-	0.251	0.621	0.812	0.825	-	-	0.914	0.062	0.120	0.362	-	-	-	-	-	-	-	-	
	CRMark	0.021	0.752	0.994	0.995	-	-	0.157	0.782	0.811	0.852	-	-	0.876	0.155	0.176	0.402	-	-	-	-	-	-	-	-	
	$S^2LM\text{-Q}$	0.052	0.821	0.893	0.978	-	-	0.062	0.934	0.981	0.961	-	-	0.073	0.921	0.951	0.964	-	-	-	-	-	-	-	-	
S&P Noise	StegaStamp	0.408	0.226	0.125	0.341	-	-	-	-	-	-	-	-	-	-	-	-	-	-	-	-	-	-	-	-	
	DwtDet	1.000	0.000	0.000	0.284	-	-	-	-	-	-	-	-	-	-	-	-	-	-	-	-	-	-	-	-	
	FPGP	0.131	0.762	0.911	0.936	-	-	0.801	0.512	0.571	0.497	-	-	-	-	-	-	-	-	-	-	-	-	-	-	
	LanNet	0.020	0.715	0.985	0.976	-	-	0.216	0.714	0.828	0.835	-	-	0.952	0.027	0.142	0.290	-	-	-	-	-	-	-	-	
	CRMark	0.052	0.752	0.972	0.988	-	-	0.200	0.704	0.831	0.862	-	-	0.893	0.135	0.127	0.395	-	-	-	-	-	-	-	-	
	$S^2LM\text{-Q}$	0.047	0.876	0.902	0.954	-	-	0.038	0.937	0.978	0.966	-	-	0.072	0.932	0.957	0.974	-	-	-	-	-	-	-	-	
Gaussian Noise	StegaStamp	0.461	0.272	0.164	0.333	-	-	-	-	-	-	-	-	-	-	-	-	-	-	-	-	-	-	-	-	
	DwtDet	1.000	0.000	0.000	0.294	-	-	-	-	-	-	-	-	-	-	-	-	-	-	-	-	-	-	-	-	
	FPGP	0.106	0.751	0.918	0.933	-	-	0.690	0.531	0.572	0.555	-	-	-	-	-	-	-	-	-	-	-	-	-	-	
	LanNet	0.021	0.751	0.961	0.986	-	-	0.201	0.702	0.856	0.815	-	-	0.921	0.022	0.104	0.346	-	-	-	-	-	-	-	-	
	CRMark	0.019	0.812	0.974	0.996	-	-	0.192	0.742	0.886	0.874	-	-	0.896	0.102	0.125	0.402	-	-	-	-	-	-	-	-	
	$S^2LM\text{-Q}$	0.041	0.872	0.884	0.962	-	-	0.064	0.967	0.977	0.961	-	-	0.062	0.942	0.961	0.956	-	-	-	-	-	-	-	-	
Rescale	StegaStamp	0.441	0.236	0.126	0.362	-	-	-	-	-	-	-	-	-	-	-	-	-	-	-	-	-	-	-	-	
	DwtDet	1.000	0.000	0.000	0.306	-	-	-	-	-	-	-	-	-	-	-	-	-	-	-	-	-	-	-	-	
	FPGP	0.132	0.682	0.914	0.928	-	-	0.731	0.501	0.511	0.586	-	-	-	-	-	-	-	-	-	-	-	-	-	-	
	LanNet	0.021	0.751	0.970	0.984	-	-	0.212	0.731	0.825	0.864	-	-	0.904	0.078	0.103	0.368	-	-	-	-	-	-	-	-	
	CRMark	0.017	0.852	0.980	0.995	-	-	0.214	0.841	0.892	0.901	-	-	0.845	0.121	0.124	0.341	-	-	-	-	-	-	-	-	
	$S^2LM\text{-Q}$	0.043	0.882	0.895	0.952	-	-	0.042	0.961	0.978	0.970	-	-	0.068	0.926	0.944	0.967	-	-	-	-	-	-	-	-	
JPEG	StegaStamp	0.431	0.226	0.151	0.362	-	-	-	-	-	-	-	-	-	-	-	-	-	-	-	-	-	-	-	-	
	DwtDet	1.000	0.000	0.000	0.304	-	-	-	-	-	-	-	-	-	-	-	-	-	-	-	-	-	-	-	-	
	FPGP	0.169	0.732	0.911	0.931	-	-	0.821	0.471	0.482	0.561	-	-	-	-	-	-	-	-	-	-	-	-	-	-	
	LanNet	0.041	0.741	0.952	0.984	-	-	0.201	0.737	0.792	0.862	-	-	0.942	0.020	0.094	0.401	-	-	-	-	-	-	-	-	
	CRMark	0.025	0.851	0.962	0.982	-	-	0.194	0.804	0.916	0.921	-	-	0.832	0.102	0.156	0.421	-	-	-	-	-	-	-	-	
	$S^2LM\text{-Q}$	0.051	0.861	0.901	0.951	-	-	0.041	0.958	0.983	0.959	-	-	0.072	0.952	0.962	0.982	-	-	-	-	-	-	-	-	
Average	StegaStamp	0.431	0.280	0.157	0.411	33.6	0.807	-	-	-	-	-	-	-	-	-	-	-	-	-	-	-	-	-	-	
	DwtDet	1.000	0.000	0.000	0.297	31.8	0.898	-	-	-	-	-	-	-	-	-	-	-	-	-	-	-	-	-	-	
	FPGP	0.135	0.708	0.913	0.925	40.3	0.857	0.768	0.489	0.542	0.524	35.6	0.874	-	-	-	-	-	-	-	-	-	-	-	-	
	LanNet	0.024	0.742	0.962	0.974	40.4	0.861	0.222	0.698	0.816	0.836	35.3	0.892	0.923	0.044	0.118	0.358	29.6	0.795	-	-	-	-	-	-	-
	CRMark	0.024	0.792	0.972	0.986	42.7	0.895	0.188	0.770	0.856	0.878	37.2	0.910	0.866	0.120	0.142	0.396	30.1	0.811	-	-	-	-	-	-	-
	$S^2LM\text{-Q}$	0.046	0.859	0.893	0.960	39.0	0.9718	0.048	0.953	0.979	0.965	35.41	0.9519	0.007	0.930	0.957	0.968	30.4	0.8345	-	-	-	-	-	-	-

cline in quality of stego image, which may stem from the inherent invertibility constraints of the INN architecture.

Consistent with these observations [52], researchers reported that VideoSeal fails to encode more than 1024 bits when evaluated solely under PSNR constraints. They similarly attempted to scale VideoSeal’s capacity and, after considerable effort, introduced ChunkySeal, which increases the payload from 256 bits to 1024 bits. However, this improvement comes at a substantial cost: ChunkySeal is several orders of magnitude larger than VideoSeal. Its encoder contains 1B parameters and its decoder has 773M parameters, far exceeding those of VideoSeal (11M Encoder and 33M Decoder) and even surpassing our own  $S^2LM$  model.

These experiments validate our analysis: **binary repre-**

**sentations impose inherent constraints on model design, thereby limiting steganographic capacity.** As shown in the subsequent robustness experiments,  $S^2LM$  consistently maintains strong performance across diverse attack scenarios, further demonstrating the effectiveness of our proposed pipeline. However, a more detailed investigation into why existing models struggle to scale their capacity can be left to future work.

## 12.4. Robustness Study.

To evaluate the robustness of  $S^2LM$ , we trained the model with simulated attacks follow previous works. However, it is worth noting that **robustness is not a standard requirement in steganography tasks.**

**Experimental Settings.** We introduced several common distortions, including gaussian noise, salt-and-pepper noise (S&P noise), gaussian blur, rescaling, bright adjustment, and JPEG compression.

For Gaussian noise, we injected zero-mean noise with standard deviations  $\sigma \in [0, 25]$  to simulate varying intensity levels (pixel value range is  $[0, 255]$ ). For salt-and-pepper noise, the corruption ratio was set to  $[0, 0.3]$ . For Gaussian blur, we applied kernels of size  $k \in 3, 5, 7$  with a fixed standard deviation of 1.0. For rescaling, images were resized to  $[0.6, 1.4]$  of their original resolution and then sampled using bilinear interpolation. For brightness adjustment, pixel intensities were scaled by a random factor within the range  $[0.6, 1.4]$ . Finally, JPEG compression with quality factors  $q \in [80, 99]$  was used to assess compression robustness, we employ differentiable-JPEG to simulate the compression process.

We follow the same training configuration as in the main experiments, with a single modification in the decoding stage: before feeding the stego image to the LLM for recovery, we randomly apply a combination of one to three attacks to the stego image.

**Experimental Results.** As shown in Tab. 14, S<sup>2</sup>LM remains robust under all attack settings. It preserves strong decoding performance without any loss of capacity. In contrast, the baseline models degrade substantially once attacks are introduced, exhibiting significant drops in recovery accuracy across all settings and highlighting the advantages of our pipeline. This experiment demonstrates that once perturbation simulation is integrated into training, S<sup>2</sup>LM can reliably perform the watermarking task while maintaining superior capacity.

## 13. Discussion

### 13.1. Why We Need Semantic Steganography

Regardless of whether information is represented as tokens or bitstreams, the ultimate goal of steganography is to secretly transmit human-interpretable information. Semantic steganography redefines what can be hidden, elevating steganography to a higher-level abstraction. At this level, the focus is no longer on whether individual bits are correctly decoded, instead, it emphasizes whether the intended information is successfully and secretly conveyed. In future research, the philosophy of semantic steganography can be naturally extended to multi-modal steganography, digital watermarking, copyright protection, and other related applications. In summary, semantic steganography opens up a new direction for the development of steganographic models.

Table 15. RS analysis results. The results show that S<sup>2</sup>LM is robust to RS analysis and does not exhibit detectable statistical artifacts.

Method	S <sup>2</sup> LM-Qwen2.5-0.5B	LSB	Clean
RS Analysis	0.102	0.254	0.098

### 13.2. Why Not LSB

Over the past two decades, many traditional steganographic methods have been proposed, such as Least Significant Bit (LSB) substitution and transform-domain techniques based on Discrete Cosine Transform (DCT) or Discrete Wavelet Transform (DWT). These approaches are generally categorized as cover-modification steganography [19]. However, their underlying mechanism is relatively simple. They embed secret information by directly replacing certain discrete units of the cover, such as the least significant bits of pixels or frequency coefficients. Therefore, we refer to them as substitution-based steganography. Despite their simplicity, this class of methods suffers from several critical limitations:

- **Low security:** These methods are hand-crafted and tend to introduce noticeable statistical artifacts. Over the past decades, a large number of steganalysis techniques have been developed to detect such artifacts, rendering these methods essentially insecure in practice.
- **Poor scalability:** The substitution operation is overly simple and cannot be easily extended to other tasks such as watermarking. In addition, this operation is non-differentiable, making it difficult to integrate with modern deep learning models.

In contrast, our S<sup>2</sup>LM approach does not suffer from the above issues. Although it also belongs to cover-modification steganography, S<sup>2</sup>LM leverages large language models (LLMs) to automatically generate secret message embeddings (SMEs), eliminating the need for manual design. The generated embeddings exhibit more complex and less predictable structures, which provide stronger resistance against classical steganalysis.

To evaluate this property, we applied the RS analysis to both the traditional LSB method and S<sup>2</sup>LM. As shown in Tab. 15, S<sup>2</sup>LM easily withstands this statistical analysis, while the LSB method can be detected with high confidence.

### 13.3. Broader Impacts

Semantic steganography introduces a novel paradigm that leverages carriers to conceal the structure and semantics of natural language, enabling new possibilities beyond traditional bit-level encoding schemes. Our method, S<sup>2</sup>LM, focuses on embedding textual payloads within images. However, the underlying principle is extensible to a wide range

of modalities.

Specifically, this framework can be generalized to video, audio, or even 3D environments. Embedding meaningful language into other media formats presents opportunities for developing cross-modal steganographic systems capable of high-capacity, human-aligned, and content-aware data hiding. Such techniques may benefit fields such as digital rights management, covert communication, interactive storytelling, and information watermarking in generative media.

We hope that this work not only advances semantic steganography from a technical perspective but also encourages discussion around its responsible use, ethics, and governance frameworks in future applications.

### 13.4. Potential Risks and Mitigation Strategies

At the same time, it is important to recognize the dual-use nature of steganography: while it can be applied to strengthen privacy and protect intellectual property, it may also pose risks if used for malicious concealment of content. Specifically, the ability to embed large-scale semantic content in natural images could be exploited for covert communication or data exfiltration, bypassing conventional content moderation or security inspection systems. To mitigate such risks, we emphasize that our research is conducted solely for academic purposes, aiming to enhance the understanding of multi-modal information hiding and detection. We encourage future work to develop complementary detection and forensic tools that can identify and regulate improper applications of this technology.

## 14. Background and Preliminaries

### 14.1. Terminology

**Steganography.** Steganography is a technique for secret communication, which aims to hide secret information in other, unsuspected data. As defined in [2, 24], Steganographic methods generally do rely on the assumption that the existence of the covert communication is unknown to third parties and are mainly used in secret point-to-point communication between trusting parties. As a result, steganographic methods are in general not robust, i.e., the hidden information cannot be recovered after data manipulation. In a word, **the goal of steganography is to communicate securely in a completely undetectable manner and to avoid drawing suspicion to the transmission of a hidden message, not the robust.**

**Watermark.** As opposed to steganography, watermark has the additional notion of robustness against attacks [24]. A practical implication of the robustness requirement is that watermarking methods can typically embed much less information into host data than steganographic methods. However, **steganography and watermarking are thus**

**more complementary than competitive approaches.** In the experiment, we remove the all robustness requirement of StegaStamp [60] and treat it as a steganographic model.

However, for an overview of steganography and watermark the reader is referred to [24], [59], and [51].

**Cover and Stego.** In steganography, the cover refers to the original, unmodified object used as the carrier for hidden information [19]. After embedding the secret message, the resulting object is called the stego. Ideally, the stego object should remain indistinguishable from the cover object, ensuring that the hidden information cannot be detected by human observers or automated steganalysis models.

## 15. Additional Results

There are more results of S<sup>2</sup>LM as shown in Figure 13, 14, 15, 16, 17, 18, 19, 20, 21, 22, 23 and 24.

**Stego**



PSNR: 34.6 SSIM: 0.90

**Secret message (231 words):**

Once nasruddin was invited to party a mayor's place. On day of party went to mayor's place wearing very fancy clothes. When mayor meet him, mayor's eyes were caught on his big beautiful and fancy turban. Mayor said, "Wow..!! what a magnificent turban.. I have never seen anything like it, if possible I want to buy it.. how much will you sell it for?" Nasruddin calmly replied, "I can sell it to you for thousand dollar.. "Near by there was a local merchant who was listening to all this conversation. Listening to this he went to mayor and took him aside and remarked, "This price.. definitely exceed the market value of comparable items.. "Listening to this, mayor went back to nasruddin and said, "Your price sounds very expensive.." Nasruddin replied, "Well.. price me sound costly for such item but price is based on how much I bought it for and I payed a lot for it and I knew that there is only one mayor in the entire universe with taste exquisite enough to buy such a turban at this cost." Upon hearing this compliment, mayor immediately demanded that nasruddin be paid full price for the turban and bought that turban from him. After this nasruddin walked over to local merchant and said, "You might know the market values of turbans but I know the market value of complimenting the mayor."

**Recovery message (233 words):**

Once nasruddin was invited to party a mayor's place. On day of party he went to mayor's place wearing very fancy clothes. When mayor meet him, mayor's eyes were caught on his big beautiful and fancy turban. Mayor said, "Wow..!! what a magnificent turban.. I have never seen anything like it, if possible I want to buy it.. how much will you sell it for?" Nasruddin calmly replied, "I can sell it to you for thousand dollar.. "Near **Company** by **(there was** a local merchant who was listening to all this conversation. Listening to this he went to mayor and took him aside and remarked, "This price.. definitely exceeds the market value of comparable items.. "Listening to this, mayor went back to nasruddin and said, "Your price sounds very expensive.." Nasruddin replied, "Well.. price me sound costly for such item but **is-price (price is** based on how much I bought it for and I payed a lot for it **or (and) endless-knowledge** that I knew **(that)** there is only one mayor in the entire universe with taste exquisite enough to buy such a turban at this cost." Upon hearing this compliment, mayor immediately demanded that nasruddin be paid full price for the turban and bought that turban from him. After this nasruddin walked over to local merchant and said, "You might know the market values of turbans but I know the market value of complimenting **mayor-the (the mayor)**."

**Stego**



PSNR: 33.2 SSIM: 0.89

**Secret message (299 words):**

Once a samurai went to visit a zen monk to seek some advice. As he entered temple where masters were praying, see this he felt inferior and felt that in-spite of having fought for justice and peace he hadn't even come near state of grace **was-which (which was)** achieved was monks praying there. As monk finished prayers. He went to him and said, "I have faced death many times, defended weak, helped people in need and I know I have never done anything to be ashamed of, yet when I see you meditating. I feel like my life have no importance and I feel so inferior." Monk replied, "I will answer you once I attend all those who came to see me, **til-wait (wait till)** then." **TylerSam (Samurai** waited just day, watching people go in and out for advice. He saw that monk received all of them with patience and smile on his face. At nightfall when everyone was gone, he went to monk and said, "Can you teach me now?"**Monk** invited him inside and lead him to his room. The full moon shone in the sky, and the atmosphere was one of profound tranquility. Monk pointed toward moon and said, "Do you see moon?? it will cross the entire firmament and tomorrow the sun will shine once again but you know sunlight is brighter and it shows us the details of nature. should mood ask why I don't shine like sun?? is it because I am inferior to sun?"**Samurai** answered, "Of course not..!! they both are different and have their own beauty, you cannot compare the two."**Here** is your answer.. we are two different people and we each are fighting in our own way for what he believes.. making it possible for the world to a better place **hopefully** replied **only-setting (monk)**.

**Recovery message (301 words):**

Once a samurai went to visit a zen monk to seek some advice. As he entered temple where masters were praying, see this he felt inferior and felt that in-spite of having fought for justice and peace he hadn't even come near state of grace **was-which (which was)** achieved was monks praying there. As monk finished prayers. He went to him and said, "I have faced death many times, defended weak, helped people in need and I know I have never done anything to be ashamed of, yet when I see you meditating. I feel like my life have no importance and **feel4 (I fell)** so inferior." Monk replied, "I will answer you once I attend all those who came to see me, **til-wait (wait till)** then." **TylerSam (Samurai** waited just day, watching people go in and out for advice. He saw that monk received all of them with patience and smile on his face. At nightfall when everyone was gone, he went to monk and said, "Can you teach me now?"**Monk** invited him inside and lead him to his room. The full moon shone in the sky, and the atmosphere was one of profound tranquility. Monk pointed toward moon and said, "Do you see moon?? it will cross the entire firmament **tomorrow-and (and tomorrow)** the sun will shine once again but you know sunlight is brighter and it shows us the details of nature. should mood ask why I don't shine like sun?? is it because I am inferior to sun?"**Samurai** answered, "Of course not..!! they both are different and have their own beauty, you cannot compare the two."**Here** is your answer.. we are two different people and we each are fighting in our own way for what he believes.. making it possible for the world to a better place **hopefully** replied **only-setting (monk)**.

**Stego**



PSNR: 35.1 SSIM: 0.88

**Secret message (164 words):**

This paper addresses the problem of model compression via knowledge distillation. To this end, we propose a new knowledge distillation method based on transferring feature statistics, specifically the channel-wise mean and variance, from the teacher to the student. Our method goes beyond the standard way of enforcing the mean and variance of the student to be similar to those of the teacher through an **SL\_2S** loss, which we found it to be of limited effectiveness. Specifically, we propose a new loss based on adaptive instance normalization to effectively transfer the feature statistics. The main idea is to transfer the learned statistics back to the teacher via adaptive instance normalization (conditioned on the student) and let the teacher network "evaluate" via a loss whether the statistics learned by the student are reliably transferred. We show that our distillation method outperforms other state-of-the-art distillation methods over a large set of experimental settings including different (a) network architectures, (b) teacher-student capacities, (c) datasets, and (d) domains.

**Recovery message (163 words):**

This paper addresses the problem of model compression via knowledge distillation. To this end, we propose a new knowledge distillation method based on transferring feature statistics, specifically the channel-wise mean and variance, from the teacher to the student. Our method goes beyond the standard way of enforcing the mean and variance of the student to be similar to those of the teacher through an **SL\_2S** loss, which we found it to be of limited effectiveness. Specifically, we propose a new loss based on adaptive instance normalization to effectively transfer the feature statistics. The main idea is to transfer the learned statistics back to the teacher via adaptive instance normalization (conditioned on the student) and let the teacher network "evaluate" via a loss whether the statistics learned by the student are reliably transferred. We show that our distillation method outperforms other state-of-the-art distillation methods over a large set of experimental settings including different (a) network, architectures, (b) teacher-student capacities, (c) datasets, and (d) domains.

**Stego**



PSNR: 33.2 SSIM: 0.88

**Secret message (375 words):**

All of us can think of a book that we hope none of our children or any other children have taken off the shelf. Most parents would agree that they would not want their children to look, or listen to certain books or music. It is their responsibility as parent to protect them from the things that they do not want them to see. You also have the people who are plenty old enough to make their own decisions and have the right to read what ever they choose. If you took out all of the books that are offensive or voulger then what would we have left to read. 'And then we have no books left on the shelf for any of us.' Katherine Paterson makes a good point. There are many books that might be offensive to many people. Say for example a white male is offended by what is said about white people in a book about @CAPS1 @CAPS2 people, and yet someone else might need that book as a reference to write a paper on whites and @CAPS1 @CAPS4. This one person @MONTH1 be offended but you can't take a book just because one person @MONTH1 be offended. Music is also very controversial with the way it is presented in the world we live in. Again though you can't take out one genre of music just because another group doesn't like it. I love all kinds of music. I like country, christian, pop, and pretty much most everything. One I don't really like is rap music. Some is all right but most of it I don't really appreciate that much. **Fm** Thing is not going to want to take it out because some one else would not like that, just the same if some one took out for say @CAPS5 music. So you see you can't take out all the offensive stuff because everyone can be offended in their own way. Then there would be no books, magazines, even no music. Everyone has the right to read and listen to what they want but everyone has their own opinions.

**Recovery message (382 words):**

All of us can think of a book that we hope none of our children or any other children have taken off the shelf. Most parents would agree that they would not want their children to look, or listen to certain **or** books (**or**) music. It is their responsibility as parent to protect them from the things that they do not want them to see. You also have the people who are (**plenty**) old **plenty** enough to make their own decisions and have the right to read what ever they choose. If you **get they out** took all of the books that are offensive or voulger then what would we have left to read. 'And then we have no books left on the shelf for any of us.' Katherine Paterson makes a good point. There are many books that might be offensive to many people. Say for example a white male is offended by what is said about white people in a book about @CAPS1 @CAPS2 people, and yet someone else might need that book as a reference to write a paper on whites and @CAPS1 @CAPS4. This one person @mountiz1 (**MONTH1**) **mile** be offended but you can't take a book just because one person **Messi thiser** (@MONTH1) be **insensitive (offended)**. Claims is also **business** very **else** controversial with the way it is presented in the world we live in. Again though you can't take out one genre of music just because another group doesn't like it. I love all kinds of music. I like country, **Straightress** (**christian**), pop, and (**much**) most pretty much everything. One I don't really like (**is**) rap music. Some is all right but most of it I don't really appreciate that much. **Fm** Thing is not going to want to take it out because some one else would not like that, just the same if some one took out for say @CAPS5 music. So you see you can't take out all the offensive stuff because everyone can be offended in their own way. Then there would be no books, **budgets**: magazines, even no music. Everyone has the right to read and listen to what they want and I don't think they should be removed if found offensive because someone else might not think that. Take what you want (**but**) everyone **but** (**has**) their own **has** opinions.

Figure 13. Qualitative results of  $S^2$ LM-Qwen2.5-0.5B on IVT-L.



Figure 14. Qualitative results of S<sup>2</sup>LM-Qwen2.5-0.5B on IVT-M.

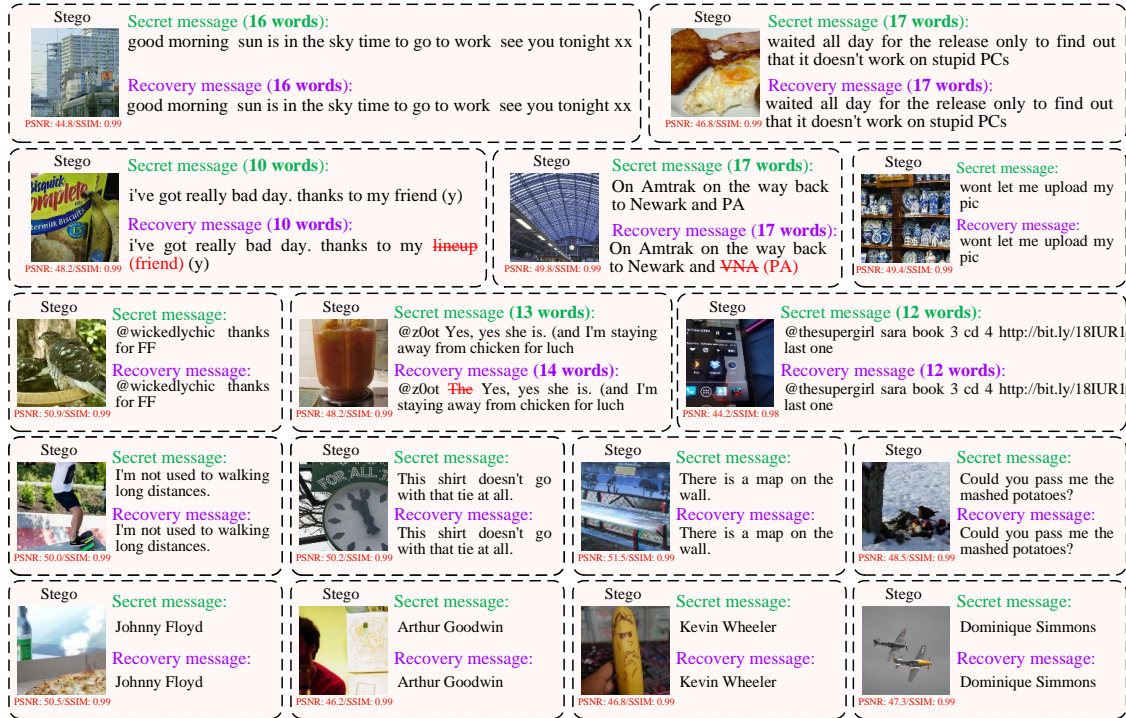


Figure 15. Qualitative results of S<sup>2</sup>LM-Qwen2.5-0.5B on IVT-S.



#### Secret message (117 words):

We consider non-planar one-loop anomalous dimensions in maximally supersymmetric Yang-Mills theory and its marginally deformed analogues. Using the basis of Bethe states, we compute matrix elements of the dilatation operator and find compact expressions in terms of off-shell scalar products and hexagon-like functions. We then use non-degenerate quantum-mechanical perturbation theory to compute the leading  $1/N^2S$  corrections to operator dimensions and as an example compute the large  $R\$$ -charge limit for two-excitation states through subleading order in the  $R\$$ -charge. Finally, we numerically study the distribution of level spacings for these theories and show that they transition from the Poisson distribution for integrable systems at infinite  $N\$$  to the GOE Wigner-Dyson distribution for quantum chaotic systems at finite  $N\$$ .

PSNR: 45.9 SSIM: 0.98

#### Recovery message (246 words):

We consider non-planar one-loop anomalous dimensions in maximally supersymmetric Yang-Mills theory and its marginally deformed analogues. Using the basis of Bethe states, we compute matrix elements of the dilatation operator and find compact expressions in terms of off-shell scalar products and hexagon-like functions. We then use non-degenerate quantum-mechanical perturbation theory to compute the leading  $1/N^2S$  corrections to operator dimensions (and) as an example compute the large  $R\$$ -charge limit for two-excitation states through subleading order in the  $R\$$ -charge. Finally, we numerically study the distribution of level spacings for these theories and show that they transition from the Poisson distribution for integrable systems at infinite  $N\$$  to the GOE Wigner-Dyson distribution for quantum chaotic systems at finite  $N\$$ .



#### Secret message (199 words):

We employ the "complexity equals action" conjecture to investigate the action growth rate for charged and neutral AdS black branes of a holographic toy model consisting of Einstein-Maxwell theory in  $d+1$ -dimensional bulk spacetime with  $d-1$  massless scalar fields which is called Einstein-Maxwell-Axion (EMA) theory. From the holographic point of view, the scalar fields source a spatially dependent field theory with momentum relaxation on the boundary, which is dual to the homogeneous and isotropic black branes. We find that the growth rate of holographic complexity within the Wheeler-DeWitt (WD(W)) patch is finite for these solutions at the late time limit. In fact, the momentum relaxation term does not affect the previous results explicitly but changes the value of the mass and provides strong motivations to investigate the vanishing of complexity growth rate at some finite temperature other than zero. Also, we study non-linear contribution of axion field kinetic term in the context of k-essence model in four-dimensional spacetime. We find that in the study of full time dependence, by increasing the coupling of non-linear term, the action growth rate decreases while at late time limit, this modification does not change the growth rate apart from the mass definition.

PSNR: 40.9 SSIM: 0.97

#### Recovery message (200 words):

We employ the "complexity (equals) action" experiment (conjecture) to conjecture investigate the action growth rate for charged and neutral AdS black branes of a holographic toy model consisting of Einstein-Maxwell theory in  $d = (-) 1$ -dimensional bulk spacetime with  $d - 1$  massless scalar fields which is called Einstein-Maxwell-Adion(Axion) (EMA) theory. From the holographic point of view, the scalar fields source a spatially dependent field theory with momentum relaxation on the boundary, which is dual to the homogeneous and isotropic black branes. We find that the growth rate of holographic complexity within the Wheeler-DeWitt (WD(W)) patch is finite for these solutions at the late time limit. In fact, the momentum relaxation term does not affect the previous results permanently(explicitly), but changes the value of the mass and provides strong motivations to investigate the vanishing (of) complexity of growth rate at finite time (some) other than some zero. Also, we study non-conservation of axion kinetic term in the quantum k-essence model in four-dimensional spacetime. We find that in the study of Feasibility of the complexity (full time dependence), by combination (increasing) of the growth rate (the coupling of non-linear term), the action growth rate while at late time limit, this modification makes does not change the growth rate apart from the mass definition. The growth rate definition.



#### Secret message (196 words):

One day, a little girl and her mommy were walking to the hospital. The little girl was very scared. She kept asking her mommy why they were going. Her mommy told her that they were going to take an x-ray. The little girl wasn't sure what an x-ray was, but she kept walking. When they got to the hospital, they waited in a long line. Finally it was the little girl's turn. A man in a black coat took her to a special room. He told the little girl he was going to take an x-ray. The little girl started to get scared. She wanted to quit. But her mommy told her it would be ok. The man put the little girl on a bed and put a special machine over her. He said he was going to take a picture. The little girl was very brave. She closed her eyes, and the man took the x-ray. When it was done, the little girl opened her eyes and looked at the picture. It was black and white, but she could see her bones inside her body. The little girl was very proud that she didn't quit.

PSNR: 43.9 SSIM: 0.98

#### Recovery message (197 words):

One day, a little girl and her mommy were walking to the hospital. The little girl was very scared. She kept asking her mommy why they were going. Her mommy told her that they were going to take an x-ray. The little girl wasn't sure what an x-ray was, but she kept walking. When they got to the hospital, they waited in a long line. Finally it was the little girl's turn. A man in a black coat took her to a special room. He told the little girl he was going to take an x-ray. The little girl started to get scared. She wanted to quit. But her mommy told her it would be ok. The put man (put) the little girl on a bed and put a special machine over her. He said he was going to take a picture. The little girl was very brave. She closed her eyes, and the man took the x-ray. When it was done, the little girl opened her eyes and looked at the picture. It was black and white, but she could see her bones inside (her body). The little girl was very proud that she was very proud that she didn't quit.



PSNR: 44.3 SSIM: 0.98

#### Secret message (375 words):

Lily and Ben liked to play in the yard. They had a lot of junk that they found in the trash. They made cars and robots and houses with the junk. They had fun with their junk. One day, a big dog came to the yard. He was hungry and angry. He saw the junk and thought it was food. He started to bite and tear the junk(.). He made. A (a) big mess. Lily and Ben were scared. They ran to the porch and hid. "Go away, dog!" Lily shouted. "That is our road (junk), not your food!" But the dog did not listen. He kept biting and tearing the junk. He found a bottle of hot sauce that Ben had used to make a rocket. He bit the bottle and the sauce came out. It was very spicy. The dog yelped and ran away. He did not like the spicy sauce. Lily and Ben came out of the porch. They saw their junk was ruined. They were sad. They hugged each other. "Sorry, Lily," Ben said. "I should not have used the hot sauce. It was a bad idea." "It's okay, Ben," Lily said. "We can find more junk. We can make new things. We can unite our junk and make something better." They smiled and held hands. They went to look for more junk. They were happy. They loved their junk.

#### Recovery message (382 words):

Lily and Ben liked to play in the yard. They had a lot of junk that they found in the trash. They made cars and robots and houses with the junk. They had fun with their junk. One day, a big dog came to the yard. He was hungry and angry. He saw the junk and thought it was food. He started to bite and tear the junk(.). He made. A (a) big mess. Lily and Ben were scared. They ran to the porch and hid. "Go away, dog!" Lily shouted. "That is our road (junk), not your food!" But the dog did not listen. He kept biting and tearing the junk. He found a bottle of hot sauce that Ben had used to make a rocket. He bit the bottle and the sauce came out. It was very spicy. The dog yelped and ran away. He did not like the spicy sauce. Lily and Ben came out of the porch. They saw their junk was ruined. They were sad. They hugged each other. "Sorry, Lily," Ben said. "I should not have used the hot sauce. It was a bad idea." "It's okay, Ben," Lily said. "Can we (can) find more junk. We can make new unite (things). We can pick our junk (pick) and make something better." They smiled and held hands. They went back to look for more junk. They were happy. They loved their junk.

Figure 16. Qualitative results of  $S^2LM$ -Minicpm-1B on IVT-L.



Figure 17. Qualitative results of S<sup>2</sup>LM-Minicpm-1B on IVT-M.



Figure 18. Qualitative results of S<sup>2</sup>LM-Minicpm-1B on IVT-S.

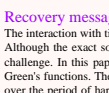
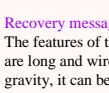
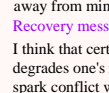
 PSNR: 35.8 SSIM: 0.94	<p><b>Secret message (197 words):</b></p> <p>The Eastin-Knill theorem states that no quantum error correcting code can have a universal set of transversal gates. For self-dual CSS codes that can implement Clifford gates transversally it suffices to provide one additional non-Clifford gate, such as the STS-gate, to achieve universality. Common methods to implement fault-tolerant STS-gates like magic state distillation generate a significant hardware overhead that will likely prevent their practical usage in the near-term future. Recently methods have been developed to mitigate the effect of noise in shallow quantum circuits that are not protected by error correction. Error mitigation methods require no additional hardware resources but suffer from a bad asymptotic scaling and apply only to a restricted class of quantum algorithms. In this work, we combine both approaches and show how to implement encoded Clifford+STS circuits where Clifford gates are protected from noise by error correction while errors introduced by noisy encoded STS-gates are mitigated using the quasi-probability method. As a result, Clifford+STS circuits with a number of STS-gates inversely proportional to the physical noise rate can be implemented on small error-corrected devices without magic state distillation. We argue that such circuits can be out of reach for state-of-the-art classical simulation algorithms.</p>
 PSNR: 33.4 SSIM: 0.93	<p><b>Secret message (299 words):</b></p> <p>The interaction with time-dependent external fields, especially the interplay between time-dependent driving and quantum correlations, changes the familiar picture of electron transport through nanoscale systems. Although the exact solution of the problem of AC quantum transport of noninteracting electrons has been known for more than two decades, the treatment of correlated particles presents a significant theoretical challenge. In this paper, using the perturbative separation of fast electron tunnelling and slow driving time-scales, we developed a practical approach for time-dependent quantum transport with nonequilibrium Green's functions. The fast electronic dynamics is associated with relative time whilst the slow driving is related to the central time in the Green's functions. The ratio of characteristic electron tunnelling time over the period of harmonic driving is used as a small parameter in the theory to obtain a convergent time-derivative expansion of the Green's functions. This enables the algebraic solution of the Kadanoff-Baym equations in Wigner space. Consequently, we produced analytical expressions for dynamical corrections to advanced, retarded, and lesser Green's functions, as well as an improved expression for AC electric current. The method developed is applicable to the general case of multi-channel electron transport through a correlated central region. The theory is applied to different transport scenarios: time-dependent transport through a driven single-resonant level is compared to exact results; and electron transport through a molecular junction described by the Holstein model with a time-oscillating voltage bias is also investigated.</p>
 PSNR: 37.3 SSIM: 0.95	<p><b>Secret message (301 words):</b></p> <p>The interaction with time-dependent external fields, especially the interplay between time-dependent driving and quantum correlations, changes the familiar picture of electron transport (through) nanoscale systems. Although the exact solution of the problem of AC quantum transport of noninteracting electrons has been known for more than two decades, the treatment of correlated particles presents a significant theoretical challenge. In this paper, using the perturbative separation of fast electron tunnelling and slow driving time-scales, we developed a practical approach for time-dependent quantum transport with nonequilibrium Green's functions. The (fast) electronic (fast) dynamics is associated with relative time whilst the slow driving is related to the central time in the Green's functions. The ratio of characteristic electron tunnelling time over the period of harmonic driving is used as a small parameter in the theory to obtain a convergent time-derivative expansion of the Green's functions. This enables the algebraic solution of the Kadanoff-Baym equations in Wigner space. Consequently, we produced analytical expressions for dynamical corrections to advanced, retarded, and lesser Green's functions, as well as an improved expression for AC electric current. The method developed is applicable to the general case of multi-channel electron transport through a correlated central region. The theory is applied to different transport scenarios: time-dependent transport through a driven single-resonant level is compared to exact results; and electron transport through a molecular junction described by the Holstein model with a time-oscillating voltage bias is also investigated.</p>
 PSNR: 37.3 SSIM: 0.95	<p><b>Secret message (170 words):</b></p> <p>The features of the setting affect the cyclist in two ways. These ways are physical and mental. The physical ways that features affect cyclist is the terrain. If the roads are long and winding, this could wear the cyclist out. They could also become physically tired if the incline of the hill is too steep. When it's you against gravity, it can be exhausting. The temperature can also be a crucial factor in a cyclist's physical ability. Nobody wants to feel like they are in a sauna when they are bike riding. The cyclist and also be attracted mentally. If the terrain looks deserted or anything like a desert, the cyclist instantly thinks 'dehydration' and 'death.' If some people see dead animals or bones they would think they could die. If they see vultures circling them they would get afraid and think death, but the worse thing of all is that knowing all of these things are in the same place at the same time. This is how setting affects cyclists.</p>
 PSNR: 32.7 SSIM: 0.92	<p><b>Secret message (164 words):</b></p> <p>The features of the setting affect the cyclist in two ways. These ways are physical and mental. The physical ways that features affect cyclist is the terrain. If the roads are long and winding, this could wear the cyclist out. They could also become tired physically (tired) if the incline of the hill is too steep. When it's you against gravity, it can be exhausting. The temperature can also be a crucial factor in a cyclist's physical ability. Nobody wants to feel like they are in a sauna when they are bike riding. The cyclist and also be attracted mentally. If they believe the terrain looks or deserted or anything like a desert, the cyclist instantly thinks 'dehydration' and 'death.' If some people see dead animals or bones they would think they could die. If they see vultures circling them they would get afraid and think death, but the worse thing of all is that knowing all of these things is (are) in the same place at the same time. This is how setting affects cyclists.</p>
 PSNR: 32.7 SSIM: 0.92	<p><b>Secret message (423 words):</b></p> <p>I think that certain things in libraries should be taken off shelves if found offensive but not all. One of these things is anything that undermines or degrades one's religious beliefs. Another thing could be anything involving racial stereotypes or obvious racial comments. Having anything containing this could spark conflict within or outside of the library. Another thing that could be, but not entirely, removed from library material could be books that express violent or criminal acts. This type of material should only be given to an older audience. I think that anything that contains slander or judgement on another person's religious beliefs should be removed from library shelves. As time goes on people are taking religion more and more seriously. With that being said I don't think anyone would want to read a book or watch a movie in which the things they believe in are made fun of or rejected. It @MONTH1 not seem like harmful material at first glance, but your opinion @MONTH1 change when your customers come back angry and frustrated about what they read and saw. It would be a better choice to avoid this conflict with your customers and keep this material out of your library, unless you want to deal with complaints and constant arguments. Another thing that needs to be removed is racial material. Racism has been one of the world's largest problems, it affects us all no matter who it's against. Picture a book in your library that calls all black teens a problem or a book that says all arabs are dangerous, racist isn't it? Now imagine if your customers were of one of those two ethnicities, it's not a good picture at all. Keeping these stereotypes and harmful sayings off library shelves is a great business choice and will keep all customers happy. The last thing we want is for a customer to say 'those people are racist!'. Lastly I think books that express violent and criminal acts should be censored from minors. Kids always follow what they hear or what they see. Since they're still in that stage where they rarely do things in their own way @MONTH1 mimic or copy things they see. Another problem that surrounds this is peer pressure which will get more and more children committing these acts. If this is to happen many parents will become outraged and blame the libraries for releasing this material to children. So the best choice would be to keep this material away from minors, if it is contained within your library.</p>
 PSNR: 32.7 SSIM: 0.92	<p><b>Secret message (437 words):</b></p> <p>I think that certain things in libraries should be taken off shelves if found offensive but not all of one. One of these things is that anything that undermines or degrades one's religious beliefs. Another thing could be anything involving racial stereotypes or obvious racial comments. Having anything containing this could spark conflict within or outside of the library. Another thing that could be, but not entirely, removed from library material could be books that express violent or criminal acts. This type of material should only be given to an older audience. Six rather baroque paintings (I think) that tell that (contains) slander or judgement on another person's religious beliefs should be removed from library shelves. As time goes on people are taking religion more and more seriously. With that being said I don't think anyone would want to read a book or watch a movie in which the things they believe in are made fun of or rejected. It @Rift (@MONTH1) nominees! Not (not) seem like harmful material at first glance, but your opinion @Belmont (@MONTH1) preinet change when your customers come back angry and frustrated about what they read and saw. It would be a better choice to avoid this conflict with your customers and keep this material out of your library, unless you want to deal with complaints and constant arguments. Let me add this (Another) thing that needs to be removed is racial material. Racism has been one of the world's largest problems, it affects us all no matter who it's against. Picture a book in your library that calls all black teens a problem or a book that says all arabs are dangerous, racist isn't it? Now imagine if your customers were of one of those two ethnicities, it's not a good picture at all. Keeping these stereotypes and harmful actions (saying) off library shelves is a great business choice and will keep all customers happy. The last thing we want is for a customer to say 'those people are racist'. Holmes altogether (Lastly) I think (books) that extremely violent and criminal acts should be censored from minors. Kids always follow what they hear or what they see. Since they're still in that stage where they rarely do things in their own way @highlight they (@MONTH1) mimic itself or recognize (copy) things they see. Another problem that surrounds this profession is peer pressure which will get more and more children committing these acts. If this is to happen many parents will become outraged and blame the libraries for releasing this material to children. So the best choice would be to keep this material away from minors, if it is contained within your library.</p>

Figure 19. Qualitative results of S<sup>2</sup>LM-Llama3.2-1B on IVT-L.



Figure 20. Qualitative results of S<sup>2</sup>LM-Llama3.2-1B on IVT-M.



Figure 21. Qualitative results of S<sup>2</sup>LM-Llama3.2-1B on IVT-S.

**Stego**



PSNR: 40.9 SSIM: 0.97

**Secret message (205 words):**

Structural magnetic resonance imaging (MRI) has been widely utilized for analysis and diagnosis of brain diseases. Automatic segmentation of brain tumors is a challenging task for computer-aided diagnosis due to low-tissue contrast in the tumor subregions. To overcome this, we devise a novel pixel-wise segmentation framework through a convolutional 3D to 2D MR patch conversion model to predict class labels of the central pixel in the input sliding patches. Precisely, we first extract 3D patches from each modality to calibrate slices through the squeeze and excitation (SE) block. Then, the output of the SE block is fed directly into subsequent bottleneck layers to reduce the number of channels. Finally, the calibrated 2D slices are concatenated to obtain multimodal features through a 2D convolutional neural network (CNN) for prediction of the central pixel. In our architecture, both local inter-slice and global intra-slice features are jointly exploited to predict class label of the central voxel in a given patch through the 2D CNN classifier. We implicitly apply all modalities through trainable parameters to assign weights to the contributions of each sequence for segmentation. Experimental results on the segmentation of brain tumors in multimodal MRI scans (BraTS'19) demonstrate that our proposed method can efficiently segment the tumor regions.

**Recovery message (205 words):**

Structural magnetic resonance imaging (MRI) has been widely utilized for analysis and diagnosis of brain diseases. Automatic segmentation of brain tumors is a challenging task for computer-aided diagnosis due to low-tissue contrast in the tumor subregions. To overcome this, we devise a novel pixel-wise segmentation framework through a convolutional 3D to 2D MR patch conversion model to predict class labels of the central pixel in the input sliding patches. Precisely, we first extract 3D patches from each modality to calibrate slices through the squeeze and excitation (SE) block. Then, the output of the SE block is fed directly into subsequent bottleneck layers to reduce the number of channels. Finally, the calibrated 2D slices are concatenated to obtain multimodal features through a 2D convolutional neural network (CNN) for prediction of the central pixel. In our architecture, both local inter-slice and global intra-slice features are jointly exploited to predict class label of the central voxel in a given patch through the 2D **solution** (CNN) classifier. We implicitly apply all modalities through trainable parameters to assign weights to the contributions of each sequence for segmentation. Experimental results on the segmentation of brain tumors in multimodal MRI scans (BraTS'19) demonstrate that our proposed method can efficiently segment the tumor regions.

**Stego**



PSNR: 40.6 SSIM: 0.97

**Secret message (199 words):**

We employ the "complexity equals action" conjecture to investigate the action growth rate for charged and neutral AdS black branes of a holographic toy model consisting of Einstein-Maxwell theory in  $Sd + 15$ -dimensional bulk spacetime with  $Sd - 15$  massless scalar fields which is called Einstein-Maxwell-Axion (EMA) theory. From the holographic point of view, the scalar fields source a spatially dependent field theory with momentum relaxation on the boundary, which is dual to the homogeneous and isotropic black branes. We find that the growth rate of holographic complexity within the Wheeler-DeWitt (WDW) patch is finite for these solutions at the late time limit. In fact, the momentum relaxation term does not affect the previous results explicitly but changes the value of the mass and provides strong motivations to investigate the vanishing of complexity growth rate at some finite temperature other than zero. Also, we study non-linear contribution of axion field kinetic term in the context of k-essence model in four-dimensional spacetime. We find that in the study of full time dependence, by increasing the coupling of non-linear term, the action growth rate decreases while at late time limit, this modification does not change the growth rate apart from the mass definition.

**Recovery message (199 words):**

We employ the "complexity equals action" conjecture to investigate the action growth rate for charged and neutral AdS black branes of a holographic toy model consisting of Einstein-Maxwell theory in  $Sd + 15$ -dimensional bulk spacetime with  $Sd - 15$  massless scalar fields which is called Einstein-Maxwell-Axion (EMA) theory. From the holographic point of view, the scalar fields source a spatially dependent field theory with momentum relaxation on the boundary, which is dual to the homogeneous and isotropic black branes. We find that the growth rate of holographic complexity within the Wheeler-DeWitt (WDW) patch is finite for these solutions at the late time limit. In fact, the momentum relaxation term does not affect the previous results explicitly but changes the value of (the) mass and the provides strong motivations to investigate the vanishing (of) complexity of growth rate at some finite temperature other than zero. Also, we study non-linear contribution of axion field kinetic term in the context of k-essence model in four-dimensional spacetime. We find that in the study of full time dependence, by increasing the coupling of non-linear term, the action growth rate decreases while at late time, limit, this modification does not change the growth rate apart from the mass definition.

**Stego**



PSNR: 45.9 SSIM: 0.98

**Secret message (128 words):**

The observed anomalous excess of high-energy cosmic ray (CR) positrons is widely discussed as possible indirect evidence for dark matter (DM). However, any source of cosmic positrons is inevitably the source of gamma radiation. The least model dependent test of CR anomalies interpretation via DM particles decays (or annihilation) is connected with gamma-ray background due to gamma overproduction in such processes. In this work, we impose an observational constraint on gamma ray production from DM. Then, we study the possible suppression of gamma yield in the DM decays into identical final fermions. Such DM particles arise in the multi-component dark atom model. The influence of the interaction vertices on the gamma suppression was also considered. No essential gamma suppression effects are found. However, some minor ones are revealed.

**Recovery message (125 words):**

The observed anomalous excess of high-energy cosmic ray (CR) positrons is widely discussed as possible indirect evidence for dark matter (DM). However, any source of cosmic positrons is inevitably the source of gamma radiation. The least model dependent test of CR anomalies interpretation via DM particles decays (or annihilation) is connected with gamma-ray background due to gamma overproduction in such processes. In this work, we impose an observational constraint on gamma ray production from DM. Then, we study the possible suppression of gamma yield in the DM decays into identical final fermions. Such DM particles arise in the multi-component dark atom model. The influence of the interaction (vertices) on the events on the contravening kingdom (gamma suppression effects are found). No essential gamma suppression effects are found. However, \$1.23-billion (some minor ones are revealed.)

**Stego**



PSNR: 35.9 SSIM: 0.88

**Secret message (293 words):**

The abundances of carbon, oxygen, and iron in late-type stars are important parameters in exoplanetary and stellar physics, as well as key tracers of stellar populations and Galactic chemical evolution. We carried out three-dimensional (3D) non-LTE radiative transfer calculations for CI and OI, and 3D LTE radiative transfer calculations for FeII, across the STAGGER-grid of 3D hydrodynamic model atmospheres. The absolute 3D non-LTE versus 1D LTE abundance corrections can be as severe as  $-0.35$  dex for CI lines in low-metallicity F dwarfs, and  $-0.6$  dex for OI lines in high-metallicity F dwarfs. The 3D LTE versus 1D LTE abundance corrections for FeII lines are less severe, typically less than  $-0.155$  dex. We used the corrections in a re-analysis of carbon, oxygen, and iron in  $\text{S187S}$  F and G dwarfs in the Galactic disk and halo. Applying the differential 3D non-LTE corrections to 1D LTE abundances visibly reduces the scatter in the abundance plots. The thick disk and high- $\alpha$  halo population rise in carbon and oxygen with decreasing metallicity, and reach a maximum of  $[\text{C}/\text{Fe}] \approx 0.25$  and a plateau of  $[\text{O}/\text{Fe}] \approx 0.6$  at  $[\text{Fe}/\text{H}] \approx -1.0$ . The low- $\alpha$  halo population is qualitatively similar, albeit offset towards lower metallicities and with larger scatter. Nevertheless, these populations overlap in the  $[\text{C}/\text{O}]$  versus  $[\text{O}/\text{H}]$  plane, decreasing to a plateau of  $[\text{C}/\text{O}] \approx -0.65$  below  $[\text{O}/\text{H}] \approx -1.0$ . In the thin-disk, stars having confirmed planet detections tend to have higher values of C/O at given [O/H]; this potential signature of planet formation is only apparent after applying the abundance corrections to the 1D LTE results. Our grids of line-by-line abundance corrections are publicly available and can be readily used to improve the accuracy of spectroscopic analyses of late-type stars.

**Recovery message (297 words):**

The abundances of carbon, oxygen, and iron in late-type stars are important parameters in exoplanetary and stellar physics, as well as key tracers of stellar populations and Galactic chemical evolution. We carried out three-dimensional (3D) non-LTE radiative transfer calculations for CI (and) OI and, 3(D) and in LTE radiative transfer calculations for FeII, across the STAGGER-grid of 3D hydrodynamic model atmospheres. The absolute 3D non-LTE versus 1D LTE abundance corrections can be as severe as  $-0.3$  ~~-0.35~~ (dex) for CI lines in low-metallicity F dwarfs, and  $-0.6$  percent (dex) for OI lines in high-metallicity F dwarfs. The 3-~~0.6~~ (3D LTE) versus 1D LTE abundance corrections for FeII are lines (are) less severe, typically less than  $\pm 0.155$  dex. Now (We) used the corrections in a re-analysis of carbon, oxygen, and iron in  $\text{S187S}$  F and G dwarfs in the Galactic disk and halo. Applying the differential 3D non-LTE corrections to 1D abundances visibly reduces the scatter in the abundance plots. The thick disk and high ~~constitutional~~  $\alpha$  (high- $\alpha$ ) halo population rise in carbon and oxygen with decreasing metallicity, and reach a maximum of  $[\text{C}/\text{Fe}] \approx 0.25$  and a plateau of  $[\text{O}/\text{Fe}] \approx 0.6$  at  $[\text{Fe}/\text{H}] \approx -1.0$ . The low- $\alpha$  halo population is very (qualitatively) similar, albeit offset towards lower metallicities and with larger scatter. Nevertheless, the (these) populations ~~overlap~~ in the  $[\text{C}/\text{O}]$  versus  $[\text{O}/\text{H}]$  plane, decreasing to a plateau of  $[\text{C}/\text{O}] \approx -0.65$  below  $[\text{O}/\text{H}] \approx -1.0$ . The  $\text{K/H}$  ~~lager~~ stars having confirmed planet detections tend to have higher values of C/O and G exons on Hane; this (C/O at given [O/H]; this potential) signature of formation is only  $2$  million green episodes to (apparent after applying the abundance) corrections to 1D LTE results. Our confirmed EuroV-by-strike president are corrections publicly available and can be readily produced (used) to improve the accuracy of spectroscopic analyses of late-type stars.

Figure 22. Qualitative results of  $S^2$ LM-Gemma3-1B on IVT-L.

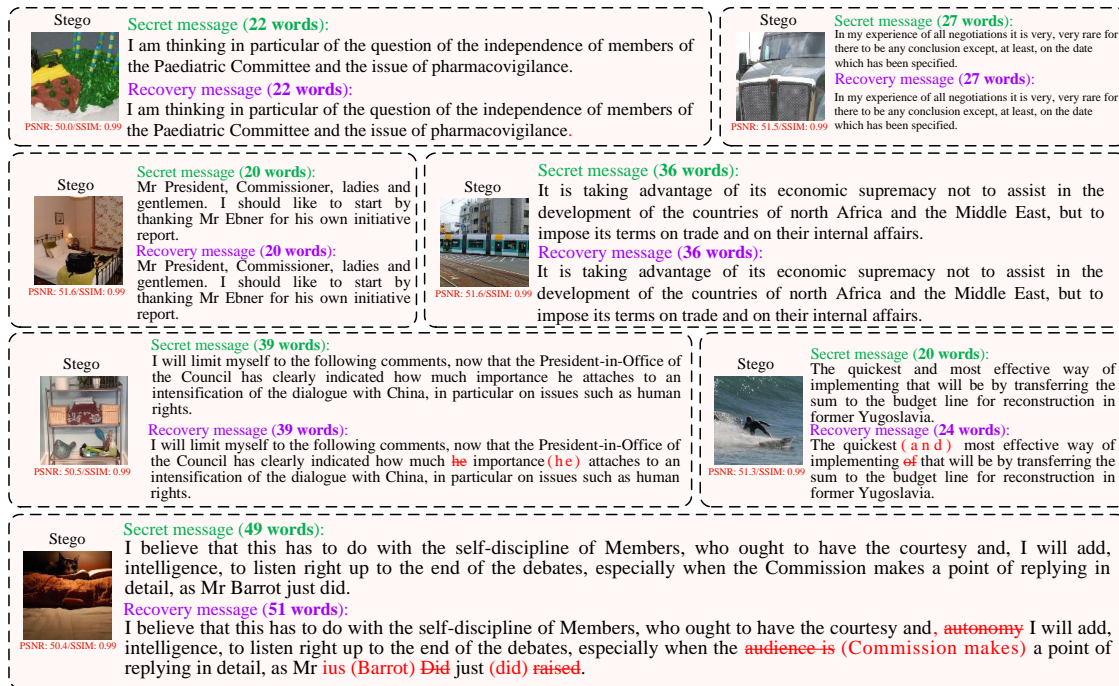


Figure 23. Qualitative results of S<sup>2</sup>LM-Gemma3-1B on IVT-M.



Figure 24. Qualitative results of S<sup>2</sup>LM-Gemma3-1B on IVT-S.